Spring 2016

Effect of build parameters on mechanical properties of ultem 9085 parts by fused deposition modeling

Krishna Prasanth Motaparti

Department:

EFFECT OF BUILD PARAMETERS ON MECHANICAL PROPERTIES OF ULTEM 9085 PARTS BY FUSED DEPOSITION MODELING

by

KRISHNA PRASANTH MOTAPARTI

A THESIS

Presented to the Faculty of the Graduate School of the

MISSOURI UNIVERSITY OF SCIENCE AND TECHNOLOGY

In Partial Fulfillment of the Requirements for the Degree

MASTER OF SCIENCE IN MECHANICAL ENGINEERING

2016

Approved by:

Ming C. Leu, Advisor
K. Chandrashekhara
Lokeswarappa R. Dharani

ABSTRACT

Additive manufacturing is a fabrication technique that is used to build components by depositing material in a layer-by-layer manner. Fused Deposition Modeling (FDM) is one of the additive manufacturing techniques which is widely used for prototyping and production applications of thermoplastic components. In load bearing applications, the flexural and compression forces often coexist. In order to avoid failure under these loads, it is essential to study the mechanical properties of the components fabricated by FDM. The main focus of this research is to study the mechanical properties of the fabricated components and to comprehend their dependence on various build parameters. It has been observed from a series of flexural and compression tests that the parts fabricated by FDM have anisotropic properties and this anisotropy was not due to the material in use, but due to the fabrication process itself. In this thesis study, Ultem 9085 material was used to fabricate coupons with variation in build parameters which include build direction, raster angle and air gap. A full factorial experimental design was used to study the individual and combined effects of these build parameters on the mechanical properties of the coupons. Solid and sparse build styles were used for coupon fabrication. Mechanical properties investigated include flexural yield strength, flexural modulus, flexural strength/mass ratio, compressive yield strength, compressive modulus and compressive strength /mass ratio. An experiment-based qualitative reasoning is used to comprehend how the mechanical properties are affected by build parameters.

ACKNOWLEDGEMENTS

First, I would like to express my deepest gratitude towards my advisor, Dr. Ming C. Leu, for his advice, support and guidance throughout my graduate studies. I would like to thank Dr. K. Chandrashekhara for his constant help and advising in this research project. I would also like to thank Dr. Lokeswarappa R. Dharani for spending his time and effort as my committee member and helping me through the course of studies.

I would also like to thank Gregory Taylor and Krishna Kolan for offering help and sharing their knowledge during the course of this project. I would like to thank my fellow students Shixuan Meng, Xin Wang, Leah Mason, Prasad Suryadevara for their help and friendship throughout my graduate work.

Finally, I am deeply indebted to my mother, Sujatha Motaparti, for her support and words of encouragement during the entire duration of my studies at Missouri University of Science and Technology.

TABLE OF CONTENTS

LIST OF FIGURES

LIST OF TABLES

1. INTRODUCTION

1.1 BACKGROUND

Additive manufacturing (AM) began as a basic process to build prototypes, but recently it has spread its roots and penetrated into almost every industry and has now become one of the most profoundly accepted manufacturing techniques due to its ease and benefits of applications. The traditional manufacturing technique of CNC machining involves a subtractive principle wherein the part that needs to be fabricated initially starts from a block of material and material is removed to generate the final part. In contrast, additive manufacturing (or popularly known as 3D printing) works on an additive principle by laying down the material layer-by-layer, as needed. Because of its ease of use and ability to easily fabricate complex parts AM has revolutionized the manufacturing industry and is now a prime topic of study among many researchers.

Fused Deposition Modeling (FDM) is one of the early commercialized additive manufacturing techniques that is widely used for fabricating thermoplastic parts. Figure 1.1. shows a schematic representation of basic FDM process.

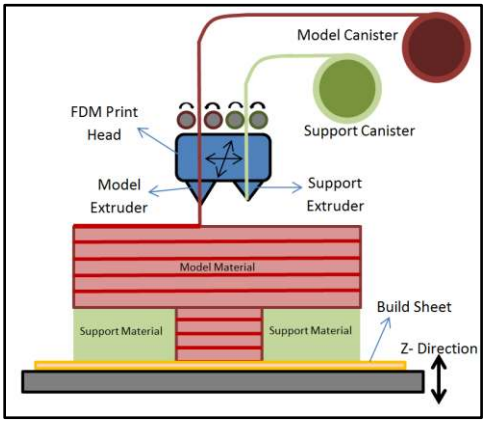

Figure 1.1. Schematic representation of FDM process

The fabrication is controlled by a machine code that is generated from a CAD model in STL (Stereo lithography) format. Once the STL file with all the predefined build parameters is sent to the FDM machine, it fabricates the physical parts by extruding

a thin bead of semi-liquefied thermoplastic material from a nozzle head that is routed back and forth horizontally on a build platform and is solidified immediately once it is extruded. In the FDM machine of our study (Fortus 400mc from Stratasys), the build platform has motion in vertical Z direction whereas the nozzle head has motion constrained to the horizontal plane (i.e. in X and Y directions). The nozzle head consists of two nozzles, one for the semi-liquefied model material and the other for support material. The support material is used to support the model material by building structures where cavities and overhangs exist in the part. This excess material can be either chemically dissolved or mechanically removed off the part.

1.2 LITERATURE REVIEW

For the past two decades, researchers have been working to study the mechanical behavior of the FDM specimens and their dependence on build parameters like build direction, raster orientation, raster width, layer thickness, oven temperature, etc. [1-10]. Schopper *et al.* [1] studied the effect of build direction on compression properties of FDM coupons and they reported that the yield strength and compressive modulus of coupons built in horizontal direction were higher in comparison to the coupons built in vertical direction. Also, according to Bagsik *et al.* [2], tensile properties of specimens made of Ultem 9085 achieved better results in all build directions using a negative air gap. Lee *et al.* [3] conducted a case study by using Taguchi approach to investigate the build parameters in order to achieve optimum elastic performance for a compliant ABS prototype. Lee *et al.* [4] compared the compressive strengths of parts made by FDM, inkjet printing and nano composite deposition system (NCDS) for different build directions. They reported that the parts made by FDM had high compressive strength in comparison to other processes. Ognzan *et al.* [5] studied the effects of layer thickness, deposition angle and infill percentage on maximum flexural force in FDM specimens made of polylactic acid (PLA) and concluded that layer thickness has the maximum effect on the flexural strength followed by the interaction between deposition angle and infill percentage. A relation between the total costs of FDM parts and mechanical properties was established by Rauta *et al.* [6] to enable the engineers to decide on proper build orientations so that the FDM parts can be fabricated with good mechanical properties at the minimum manufacturing cost. The effects of raster angle, oven

temperature, and raster width on properties of FDM parts made of ABS were studied using a bacterial foraging technique by Panda *et al.* [7] in order to suggest optimal build parameter settings to achieve good strength. Rayegani *et al.* [8] used the group method for data handling for prediction purposes and developed a functional relationship between build parameters and the part's tensile strength for the FDM process.

During the production of components using FDM, factors like build time and surface roughness play an important role. Several studies were conducted to optimize these factors with different build parameters. Anitha *et al.* [9] used Taguchi technique to study the various build parameters used in FDM that affect the quality of the fabricated prototype. The quality was measured in terms of surface roughness of the part and it was found that layer thickness, raster width and speed of deposition influence the quality of prototypes with layer thickness having the maximum effect. Similar experiments conducted by Vasudevarao *et al.* [10] revealed that part orientation also affects surface finish and air gap does not influence the surface quality much.

Literature study reveals that several experimental works have been done in evaluating the compressive and tensile properties of FDM parts by varying build parameters such as raster angle, raster width, layer thickness etc. for solid build parts. However, the previous studies analyze only the data from the experiments and do not provide much qualitative reasoning for the observed properties of parts.

1.3 MACHINE AND BUILD PARAMETERS

Fortus 400 mc (Stratasys, Eden Prairie, MN) was the machine used for the fabrication of specimens in this study.The machine has a build envelope of 406 mm x 356 mm x 4.6 mm (16" x 14" x 16") and an accuracy of ± 0.0015 mm per mm. Multiple thermoplastic materials such as ABS, ULTEM, Poly Carbonate (PC) and PPSF can be used in this machine.

ULTEM 9085 is the model material used in this study. It is a high-performance, production-grade thermoplastic with good strength to weight ratios which makes it particularly suitable for aerospace industries. A breakaway support material known as ULTEM is used alongside the model material. The mechanical properties of this material make it desirable for the study. Figure 1.2. shows the schematic of a sample layer.

The FDM process is a simple 3-stage process:

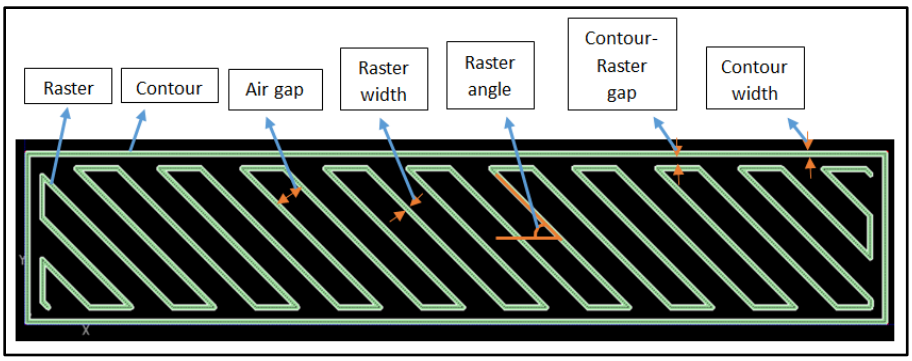

Figure 1.2. Schematic of a layer showing different build parameters

- Pre-processing: The 3D models of the coupons are modeled in SolidWorks (*in this study*) and exported as Stereo lithography (STL) file format. The STL file undergoes pre-processing during which the tool path essential for fabrication of specimens is generated after specifying various build parameters. The pre-processing of the STL file was done using Stratasys Insight 9.1 software.
- Fabrication: The STL file is then sent to the machine with the help of Stratasys Insight and Control Center Job Processing and Management software. The 3D printer begins to fabricate the part by extruding the thermoplastic material and depositing it layer by layer.
- Post-processing: After the model is fully fabricated, it is taken out of the machine and the support structures are mechanically removed by mechanically removing them off the part or chemically dissolving it to make the part ready for use.

1.4 RESEARCH OBJECTIVES

The main objectives of this research are to understand the anisotropic behavior of the thermoplastic parts built by fused deposition modeling and to study the effects of various build parameters including build direction, raster angle and negative air gap on the compressive and flexural properties of the parts fabricated by FDM.

In this study, Ultem 9085 material was used to investigate the dependence of mechanical properties (flexural and compressive) on build direction for parts fabricated with solid and sparse build styles. An experimental investigation was conducted to comprehend the behavior of FDM fabricated coupons for various parameters by qualitative reasoning with the help of optical images and physical models.

There were two sets of experiments done in this study. The first set of experiments (*presented in Section 3*) deal with the understanding of the effect of build direction on the mechanical properties of FDM fabricated coupons under three different temperatures. Using the observations from this study, a qualitative reasoning was presented (*in Section 4*) to comprehend the behavior of test coupons for different build directions. This experiment-based qualitative reasoning in Section 4 was extended to study the effects of raster angles and negative air gaps on the mechanical properties of FDM coupons. The second set of experiments (*presented in Sections 5 and 6*) deal with the effects of parameters including raster angle, negative air gap and build direction on the mechanical properties of FDM fabricated coupons at room temperature.

2. EXPERIMENTAL PROCEDURE

2.1 COUPON FABRICATION

The coupons were built with ULTEM 9085 using a Fortus 400mc machine (from Stratasys Corporation) in two build directions, namely horizontal and vertical. In the horizontal build, the build direction of the coupon is parallel to the load applied on that coupon, whereas for the vertical build the build direction of the coupon is perpendicular to the applied load. The coupons were rectangular blocks with dimensions of 127 mm x 25.4 mm x 6.35 mm (5" x 1" x 0.25") for flexural tests and 38.1 mm x 38.1 mm x 25.4 mm (1.5" x 1.5" x 1") for compression tests. The raster angle of all the fabricated coupons was kept at (45°,-45°).

The build parameters used for coupon fabrication are as follows:

- Raster width= 0.508 mm (0.02")
- Contour width= 0.508 mm (0.02")
- Air gap = 2.54 mm (0.1") (for sparse coupons)
- Raster angle = (45°,-45°)

2.2 FLEXURAL TEST

Flexural tests were conducted at three different temperatures (70F, 180F, 250F). A 3-point bend test was done according to ASTM D-790 standard on an Instron 5985 high capacity universal testing machine (Instron, Norwood, MA) at Missouri S&T. The dimensions of the flexural test coupons were 127 mm x 25.4 mm x 6.35 mm (5" x 1" x 0.25"). Figure 2.1. shows the different build vs. load directions of the flexural test coupons. In horizontal build specimens, the build direction of fabrication is parallel to the direction final flexural load applied on the specimen. Whereas, in the case of vertical specimens, the build direction of fabrication is perpendicular to the final flexural load applied on the specimen.

The test measures the flexural strength and flexural modulus of ULTEM 9085 coupons. The rate of loading used during the test was 2.54 mm/min (0.1 in/min). The 3-point bending test was carried out as shown in the Figure 2.2.

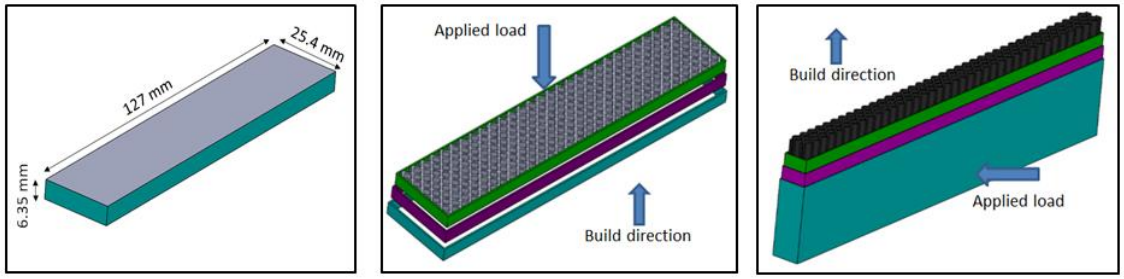

Horizontal Build Vertical Build

Figure 2.1. Dimensions and build directions of flexural test coupons

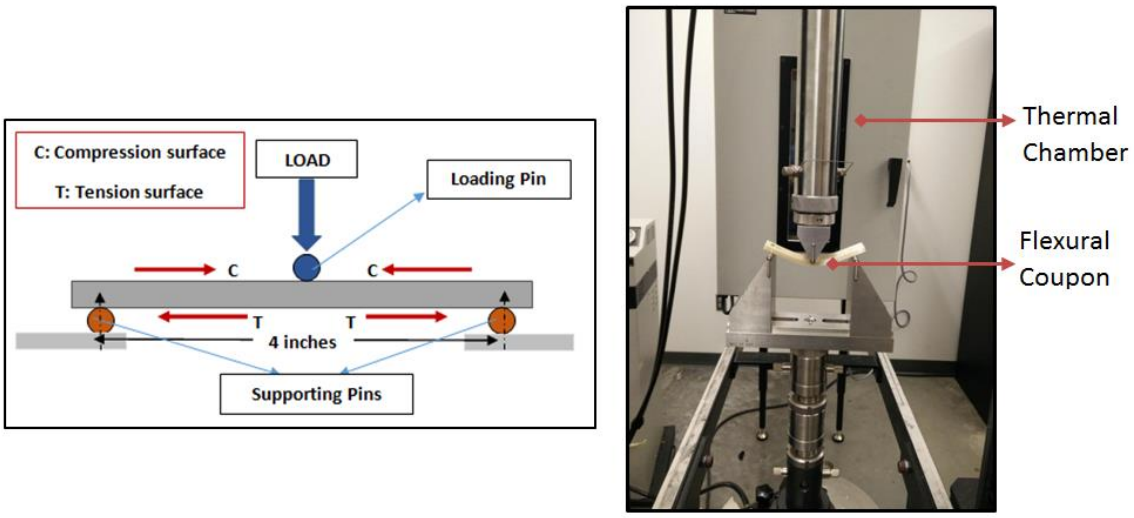

Figure 2.2. Experimental set-up: 3-point flexure test

In accordance to the test standard, the distance between the supporting pins (span length) was adjusted at 101.6 mm (4'') during our testing. The load was applied with the help of a loading pin at the center of the span length. The surface begins to bend gradually and the stress vs. strain data for the test specimen is plotted automatically by the machine. The stress caused by the bending moment in a 3-point bend test is known as flexural stress and it is calculated using Equation 1. On the other hand, flexural strain is defined as the nominal fraction change in the length of an element on the outer surface of the test specimen at mid span, where the maximum strain occurs [18]. It may be calculated for any deflection using Equation 2.

$$\sigma_f = \frac{3PL}{2bd^2} \quad \text{where, } \sigma\text{= Stress in outer fibers (MPa)} \quad (1)$$
P= Load at the midpoint (N)
L= Support span (mm)
b= Width of beam tested (mm)
d= Depth of beam tested

$$\varepsilon_f = \frac{6Dd}{L^2} \quad \text{where, } \varepsilon\text{= Strain in outer fibers (mm/mm)} \quad (2)$$
D= Maximum deflection (mm)
L= Support span (mm)
d= Depth of beam tested

As shown in Figure 2.2., the surface in contact with the loading pin (upper surface) experiences compression, whereas the surface in contact with the supporting pins (bottom surface), experiences tension. Once the maximum load is reached a crack initiates on the bottom surface and propagates towards the upper surface, thus causing the coupon to break or deform largely. The test ends once the material reaches 5% strain (even though the coupon does not break).

2.3 COMPRESSION TEST

Compression tests were conducted at three different temperatures (70F, 180F, 250F) on an Instron 5980 universal testing machine with a compression fixture. The load is applied by placing the test specimen in between the circular fixtures and compressing it slowly as shown in Figure 2.3. The machine automatically plots the compressive stress vs. compressive strain data for each test specimen. In a compression test, the stress is defined as the compressive load per unit area of the loaded cross-section with gage boundaries, carried by the test specimen at any given moment [20]. It is expressed in force per unit area as shown in Equation 3. Compressive strain is defined as the ratio of compressive deformation to the gage length of the test specimen, that is, the change in length per unit of original length along the longitudinal axis [20]. It is expressed as a dimensionless ratio as shown in Equation 4.

$$\sigma_c = \frac{F}{A} \quad \text{where, } \sigma\text{= Compressive stress (MPa)} \quad (3)$$
A= Cross-sectional area of the test specimen (mm^2)

$$\varepsilon_c = \frac{\Delta L}{L_o} \qquad (4)$$

where, ε= Compressive strain (mm/mm)
ΔL= Change in length along the longitudinal direction (mm)
L= Original length (mm)

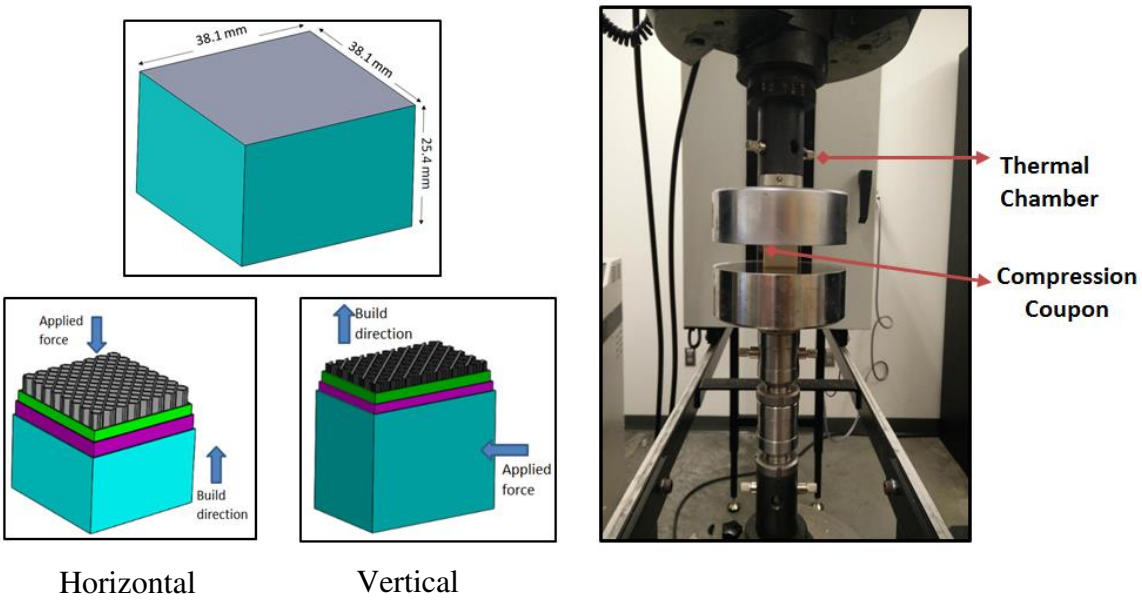

Figure 2.3. Build directions and experimental setup for compression test

The dimensions of the compression test coupons were 38.1 mm x 38.1 mm x 25.4 mm (1.5” x 1.5” x 1”). The compressive load was applied on the areas of the coupon with dimensions 38.1 mm x 38.1 mm as shown in Figure 2.3., at a constant loading rate of 1.27 mm/min (0.05 in/min). The test ends when the material reaches 10% strain. The yield strength was calculated using 0.2% offset.

3. INITIAL EXPERIMENTAL RESULTS AND OBSERVATIONS

3.1 FLEXURAL TESTING

A sample size of 5 specimens was tested for each combination of build styles and temperatures. The temperatures included 24°C (75°F), 82°C (180°F), 121°C (250°F). The mechanical properties of the samples were averaged and are presented in the Table 3.1. The mechanical properties under observation are yield strength, flexural modulus, strength/mass ratio and modulus/mass ratio. The detailed dataset obtained for calculating the averages is given in Appendix A.

Table 3.1. Mechanical properties of different build styles at three different temperatures for flexural testing. (S-H: Solid coupons with horizontal build; S-V: Solid coupons with vertical build;SP-H: Sparse coupons with horizontal build; SP-V: Sparse coupons with vertical build)

Build Styles	Raster width (mm)	Airgap (mm)	Temperature	Build Time (Min)	Yield Strength (MPa)	Flexural Modulus (MPa)	Mass (g)	Strength/Mass Ratio (MPa/g)	Modulus/Mass Ratio (MPa/g)
S-H	0.508	-	24 C	28	64.7	1875	24.04	2.69	78
SP-H	0.508	2.54		23	58	1803	18.32	3.17	98.42
S-V	0.508	-		38	87.1	2384	24.04	3.62	99.17
SP-V	0.508	2.54		32	63.4	1814	18.21	3.48	99.62
S-H	0.508	-	82 C	28	42.9	1480	24.04	1.78	61.56
SP-H	0.508	2.54		23	36.9	1315	18.32	2.01	71.78
S-V	0.508	-		38	71.7	2103	24.04	2.98	87.48
SP-V	0.508	2.54		32	47.5	1658	18.21	2.61	91.05
S-H	0.508	-	121 C	28	32.6	1317	24.04	1.36	54.78
SP-H	0.508	2.54		23	28.8	1209	18.32	1.57	65.99
S-V	0.508	-		38	57.4	1903	24.04	2.39	79.16
SP-V	0.508	2.54		32	46.6	1543	18.21	2.56	84.73

A graphical representation of the averaged properties with standard deviation is shown in Figure 3.1. It can be clearly seen that the mechanical properties of these coupons vary with both temperature and build direction.

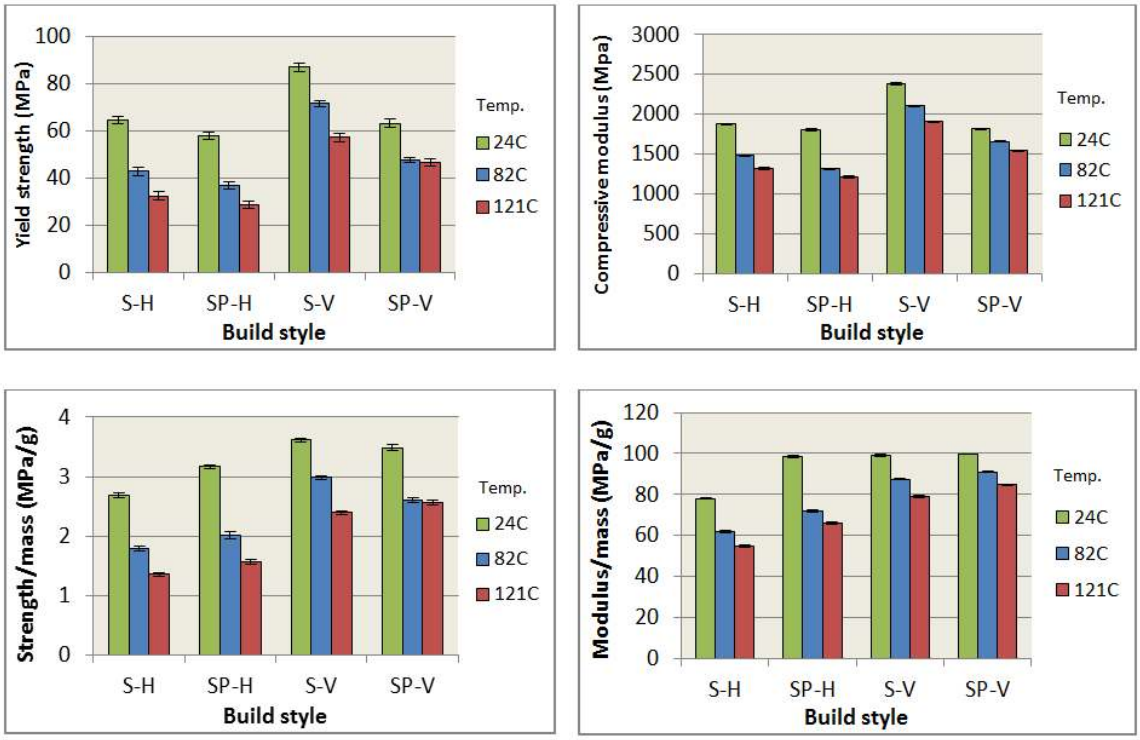

Figure 3.1. Comparison of mechanical properties for different build styles from flexural testing

From Figure 3.1., it is evident that at all three temperatures [24°C (75°F), 82°C (180°F), 121°C (250°F)], the yield strength, flexural modulus, strength/mass ratio and modulus/mass ratio of the vertical-built coupons (S-V and SP-V) are better in comparison to the corresponding horizontal-built coupons (S-H and SP-H). Also, increase in temperature leads to decrease in the mechanical properties of the coupons. The coupons with S-V build style (solid coupon with vertical build) exhibits the highest strength and modulus at all temperatures. This makes it clear that build direction affects the mechanical properties of FDM fabricated coupons. The effect of build direction is more evident in the case of solid coupons when compared to sparse coupons.

3.2 COMPRESSION TESTING

A sample size of 5 coupons was used for each combination of build styles and temperatures [24°C (75°F), 82°C (180°F), 121°C (250°F)]. The averaged values of the properties are given in Table 3.2. and the detailed data are given in Appendix B.

Table 3.2. Mechanical properties of different build styles for compression testing. (S-H: Solid coupons with horizontal build; S-V: Solid coupons with vertical build; SP-H: Sparse coupons with horizontal build; SP-V: Sparse coupons with vertical build)

Build Styles	Raster width (mm)	Airgap (mm)	Temperature	Build Time (Min)	Yield Strength (MPa)	Compression Modulus (MPa)	Mass (g)	Strength /Mass Ratio (MPa/g)	Modulus /Mass Ratio (MPa/g)
S-H	0.508	-	24 C	36	84.3	833	44.66	1.89	18.65
SP-H	0.508	2.54		25	46.1	651	26.92	1.71	24.18
S-V	0.508	-		38	63.5	828	44.66	1.42	18.54
SP-V	0.508	2.54		31	27.4	457	28.9	0.95	15.81
S-H	0.508	-	82 C	36	58.9	797	44.66	1.32	17.85
SP-H	0.508	2.54		25	34.2	575	26.92	1.27	21.36
S-V	0.508	-		38	51.3	738	44.66	1.15	16.52
SP-V	0.508	2.54		31	22.4	411	28.9	0.78	14.22
S-H	0.508	-	121 C	36	46.1	692	44.66	1.03	15.49
SP-H	0.508	2.54		25	24	491	26.92	0.89	18.24
S-V	0.508	-		38	40.3	711	44.66	0.9	15.92
SP-V	0.508	2.54		31	17.1	395	28.9	0.59	13.67

A graphical representation of data in Table 3.2. along with the standard deviation is shown in Figure 3.2.

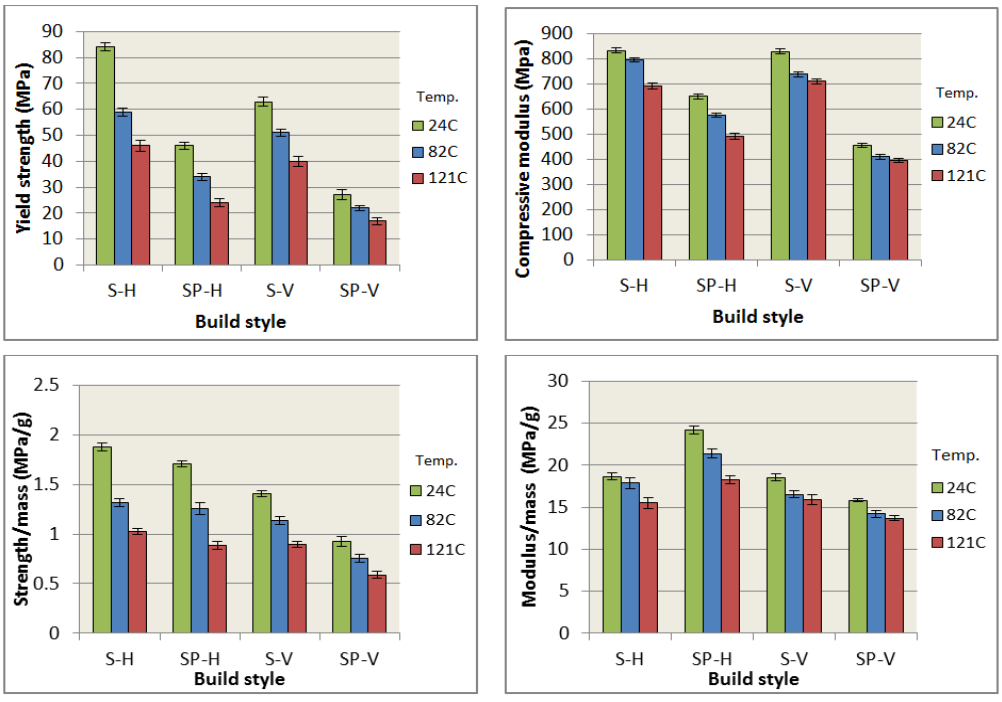

Figure 3.2. Comparison of mechanical properties for different build styles from compression testing

From this figure, it can be seen that unlike flexural test results, the mechanical properties of horizontal coupons (S-H and SP-H) are higher than those of vertical coupons (S-V and SP-V) in the case of compression. Thus, the effect of build direction (horizontal vs. vertical) is reversed in the case of compression properties compared with flexure properties.

4. INVESTIGATION OF FRACTURED SURFACE

From the experimental results it is evident that the build direction has a significant effect on both flexural and compressive mechanical properties of FDM fabricated coupons. In the flexural testing, the vertical build coupons display higher mechanical properties in comparison to the horizontal build coupons, whereas in the compression testing the horizontal build coupons display higher mechanical properties in comparison to the vertical build coupons. In order to understand these variations in mechanical properties, the fractured/deformed surfaces of the test coupons were examined under an optical microscope.

4.1 SPECIMEN PREPARATION

During the flexural testing, the coupons were tested in accordance to the ASTM D790 standard. According to the testing standard, the specimen/coupon was loaded until rupture occurred in the outer surface of the test specimen or until a maximum strain of 5% was reached, whichever occurred first. None of the coupons fractured during the testing, but were plastically deformed until reaching a standard 5% strain. In order to examine the interior structure, the coupons needed to be broken crisply. To achieve this, the coupons were treated with liquid nitrogen and then fractured. Liquid nitrogen was poured into a Styrofoam box and the coupons were held with a plier and suspended into liquid nitrogen for 4-5 minutes as shown in Figure 4.1. This exposure to liquid nitrogen made the Ultem 9085 coupons very brittle. After they were removed from the liquid nitrogen they were broken into two. Since the fracture was very brittle, there were no signs of any plastic deformation and the internal structure was clear and ready for examination.

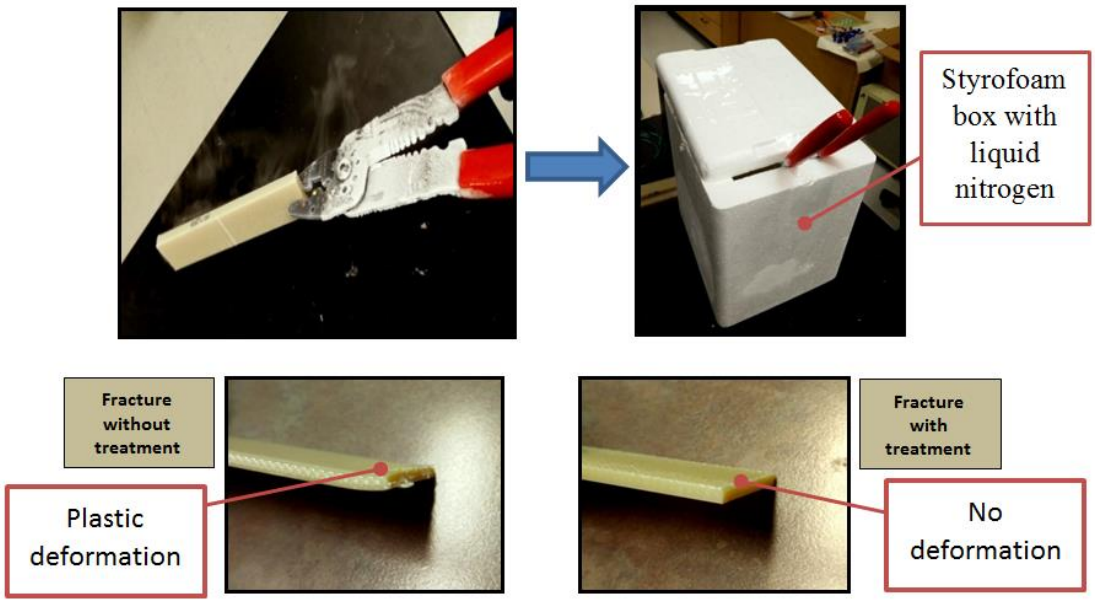

Figure 4.1. Surface fracture of the coupons with and without liquid nitrogen treatment

4.2 MICROSCOPIC EXAMINATION

After the treatment of liquid nitrogen, the specimen was broken halfway using an impact force, thus exposing its internal structure. This structure was then examined under an optical microscope. The microscope used for this purpose was Hirox KH-8700 Digital microscope. The microscopic image of the internal structure allows a good understanding of the FDM process on the bonding between the rasters after the part has been fabricated. In this case, the specimen with (0º, 90º) raster angle is examined by a microscope and the images are shown in Figures 4.2. and 4.3.

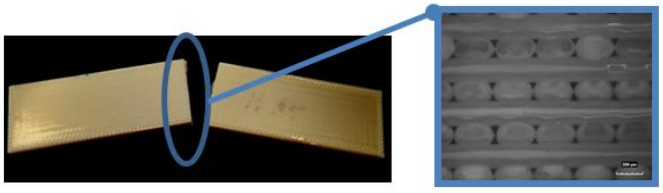

Figure 4.2. Microscopic image of the internal structure

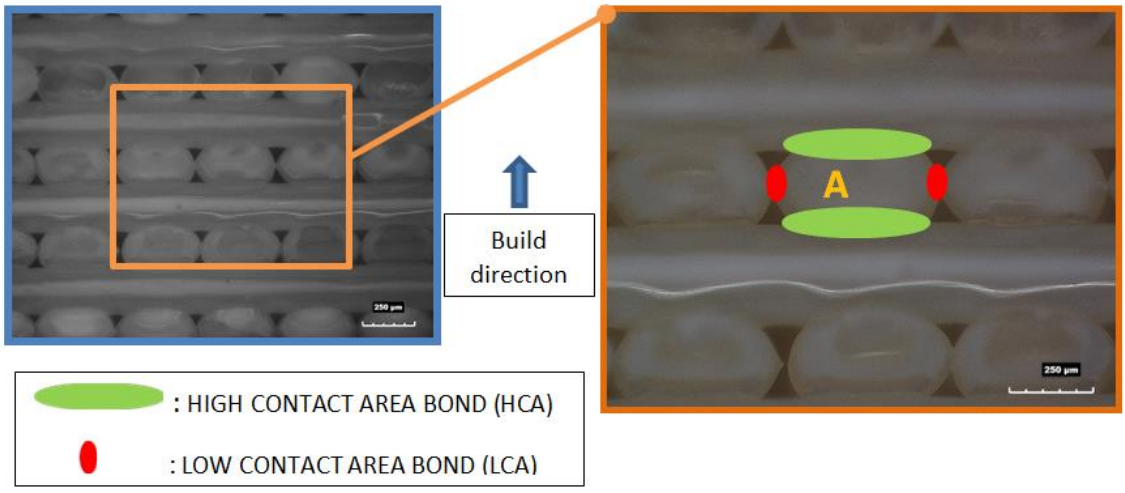

Figure 4.3. Magnified image showing the raster bonds for zero air gap rasters and (0º, 90º) raster angle

From the images in Figures 4.2. and 4.3, it can be seen that the raster (FDM beads) are elliptical in shape. This elliptical shape leads to non-uniform bonding along the circumference of the raster. For example, consider a raster 'A' in Figure 4.3. This raster has an intra-layer bonding with other rasters surrounding it. The bonding represented in green is the Higher Contact Area (HCA) bond as the area of contact between the rasters is larger in comparison to the bonding represented in red which is a Lower Contact Area (LCA) bond. HCA bonds are formed in between the layers along the direction of the build. Simply put, inter-layer bonding is HCA bonding and intra-layer bonding is LCA bonding. In general, bonds with larger areas of contact should be able to take larger forces before rupture in comparison to the bonds with smaller areas of contact.

This difference of bonding between the rasters can result in variation of mechanical properties for different build parameters. A qualitative reasoning is provided below with the help of 3D models for a clear understanding about how the variation in bonding can affect the mechanical properties.

4.3 EXPERIMENTAL INVESTIGATION

4.3.1 Flexural Test. The physical models of both horizontal and vertical flexural coupons are presented below to understand the behavior of specimens under loading.

4.3.1.1 Horizontal build – flexural coupon. In the case of horizontal build, the build direction of the coupon is parallel to the applied flexural load during the testing. A (45°, -45°) raster angle was used to fabricate the coupons. As the FDM process is a layer-by-layer fabricating process, a (45°, -45°) raster angle would mean that the first layer of rasters are printed at an angle of +45° to the horizontal axis and the next layer is printed at -45°. After the completion of each layer, the nozzle extrudes the boundary (contour) of that layer. The contours are represented in blue in Figures 4.4. and 4.5. This process of printing layers at +45° and -45° degrees continues until the desired part is fully fabricated as shown in Figure 4.5. Each layer has a constant layer thickness of 0.254 mm (0.01'').

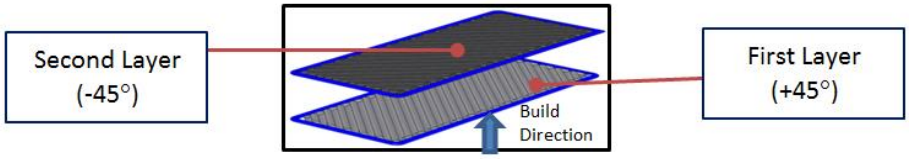

Figure 4.4. Horizontal build: +45 and -45 layer with contours

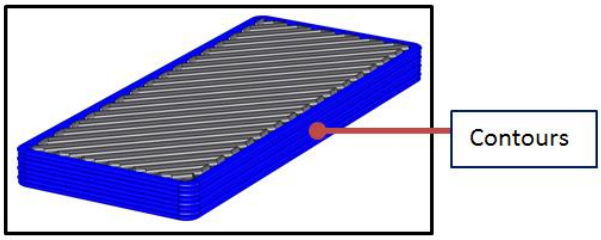

Figure 4.5. Illustration of a fully fabricated horizontal flexural coupon

After the coupon is fabricated, it is loaded in a 3 point bending test as seen in Figure 4.6. A closer look at the section view of the completely fabricated coupon would give a clearer understanding of where and how the coupon fails when the load is acting on it. As shown in Figure 4.6., the bottom surface of the coupon experiences tension and the top surface of the coupon experiences compression at the same time. Figure 4.7 shows the bottom surface which comprises of aligned rasters.

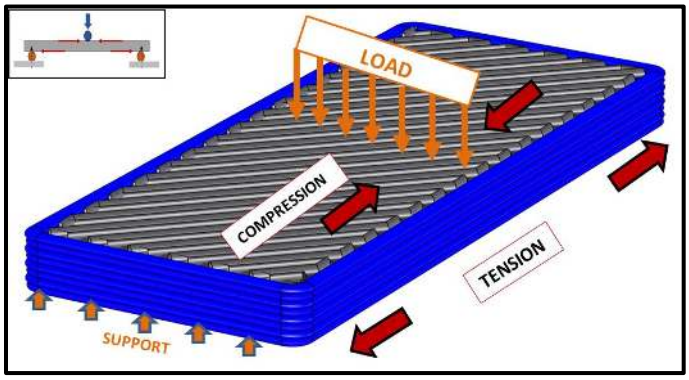

Figure 4.6. Model showing the layers under compression and tension for horizontal build

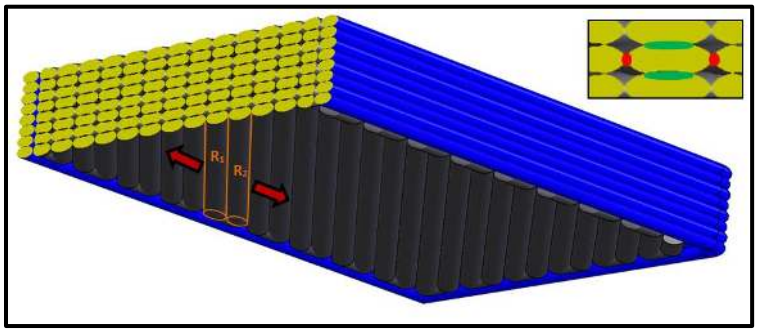

Figure 4.7. Model showing the bottom surface under tension and raster being pulled apart

As shown in Figure 4.6, the loaded coupon experiences compression and tension on its top and bottom surfaces, respectively. The surface in contact with the load (loading pin) is under compression, whereas the bottom surface in contact with the support (supporting pins) is under tension. In Figure 4.7, the section view of the coupon can be seen. The macro structure of the rasters looks similar to the ones explained earlier in Figure 4.3. The two rasters R_1 and R_2 shown here are bonded together by a LCA bond (represented in red), whereas the HCA bonds (represented in green) lie along the direction of build. Additionally, the rasters are oriented at an angle of 45° and the bottom surface with rasters R_1 and R_2 is under tension. These aligned rasters are pulled apart by rupturing the LCA bond between them and the stress propagates towards the upper surface (as shown in Figure 4.9. (A)), thus deforming the coupon and fracturing it

eventually. In the case of horizontal build coupons, the contours are on the outermost section of the coupon and do not offer much resistance to the applied load since they are not in the load bearing surfaces (upper or bottom surface). Deterioration of the bottom surface is shown in Figure 4.8.

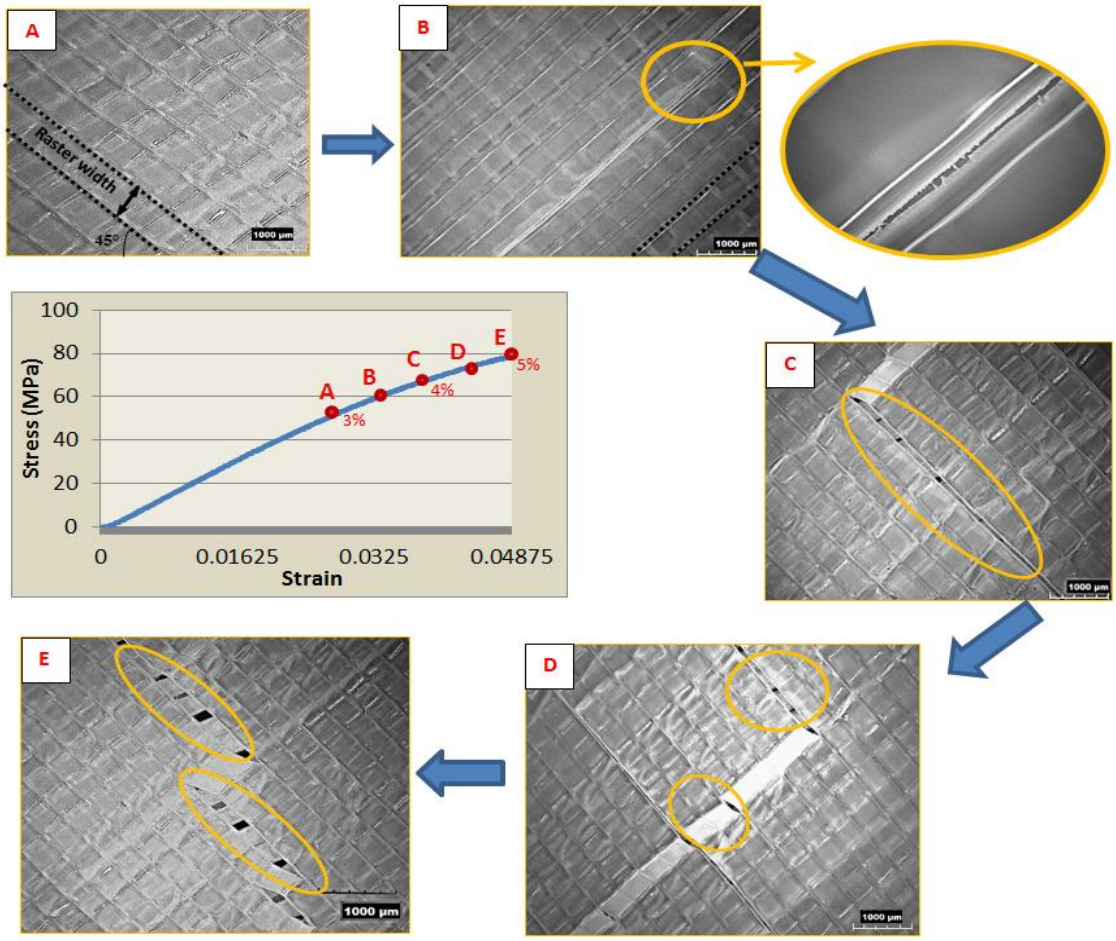

Figure 4.8. Deterioration of the bottom surface of horizontal build flexural coupons with increase in strain.

Gradual deterioration of the bottom surface of flexural coupons with horizontal build can be seen in Figure 4.8. During the 3-point bend test, the tension in the bottom surface of a flexural coupon increased continuously as the loading increased until the strain reached a standard 5% strain. Due to the increase in tension, the rasters in the bottom surface deteriorated gradually as shown in Figure 4.8. The rasters deposited at

(45°,-45°) remained intact until 3% strain (point A in the stress-strain curve) and did not show any signs of ruptures. As the strain increased to 4%, the LCA bonds between the rasters begins to deteriorate slightly and the rasters were pulled apart as shown in Figures 4.8. (B) and (C). This deterioration kept on increasing until 5% strain leading to multiple ruptures as shown in Figures 4.8. (D) and (E). Thus, the gradual deterioration of the bottom surface leads to the failure of flexural coupons as shown in Figure 4.9.

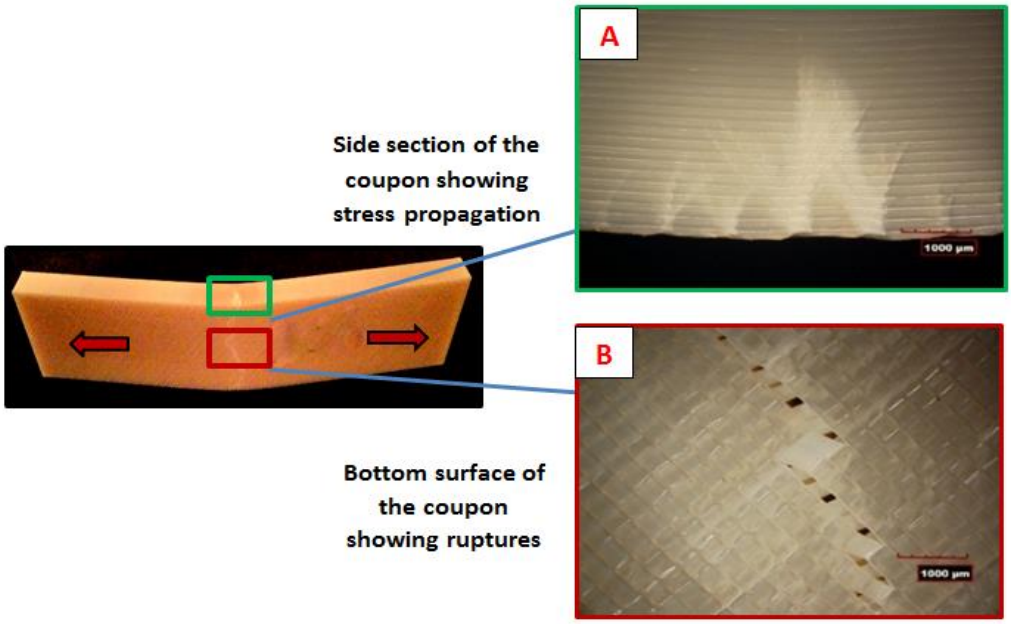

Figure 4.9. Coupon showing the ruptured surface and stress propagation at 5% strain

Figure 4.9. (A) shows the stress propagation among contours towards the upper surface of the flexural coupon at 5% strain. Figure 4.9 (B) shows the ruptured bottom surface of a flexural coupon exposing the subsequent layer at the standard 5% strain. As mentioned earlier in Figures 4.6. and 4.7., the side surface of the flexural coupon comprised of contours which were deposited one over another.

4.3.1.2 Vertical build – flexural coupon. For vertical build coupons, the build direction is perpendicular to the applied flexural load during the testing. A (45°, -45°) raster angle was used to fabricate the coupons. Similar to the horizontal build coupons, the part was fabricated by printing alternative layers at -45° and +45° angles. After the

completion of each layer, the nozzle extruded the boundary (contour) of that layer. The contours are represented in blue in Figures 4.10. and 4.11. Each layer had a constant layer thickness of 0.254 mm (0.01'').

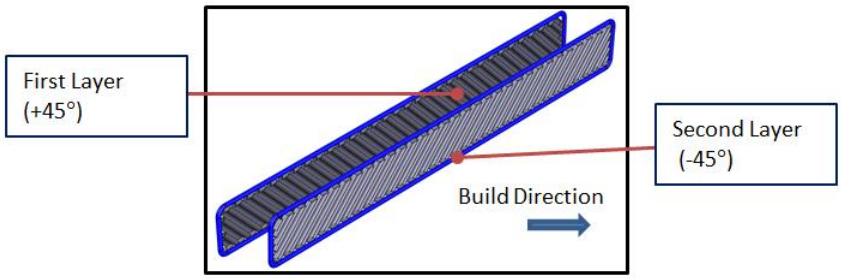

Figure 4.10. Vertical build: +45 and -45 layer with contours

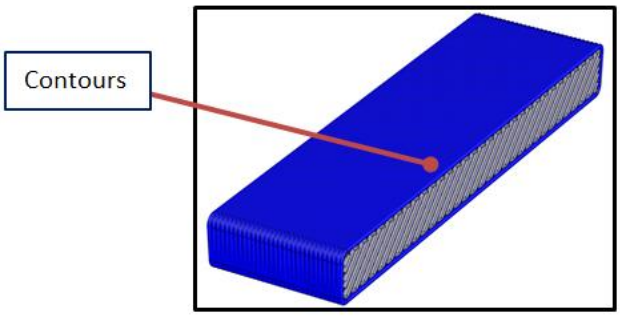

Figure 4.11. Fully fabricated vertical flexural coupon

After the coupon was fabricated, it was loaded in 3 point bending test. A closer look at the section view of the completely fabricated coupon would give a clearer understanding of where and how the coupon fails when the load is acting on it.

Once the vertical build coupon was loaded, the surface in contact with the loading pin was under compression and the bottom surface was under tension. Figure 4.12. (b) shows the cross-section of the vertical coupon. Unlike horizontal build, the contours (represented in blue) in vertical build are in the top and bottom surfaces where the stresses are the largest.

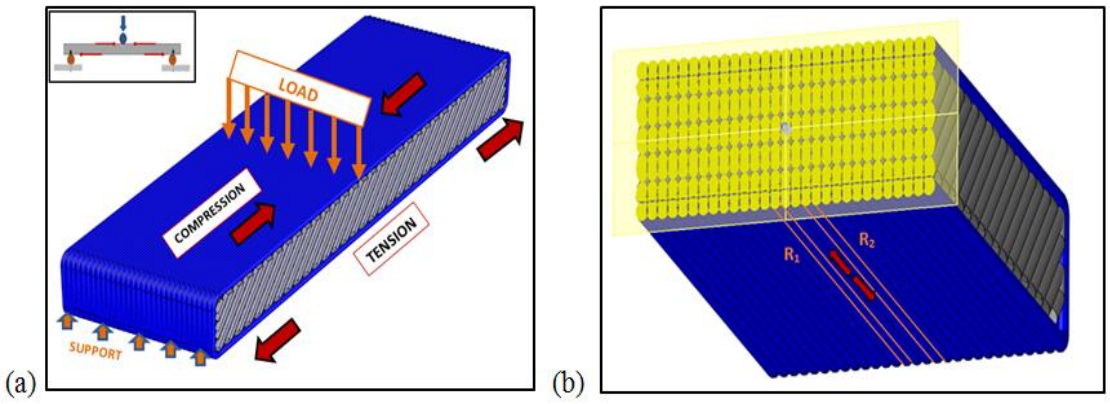

Figure 4.12. (a) Model showing the layers under compression and tension for vertical build during flexural test; (b) Tension along the length of the rasters (R_1, R_2) in the bottom surface of the coupon

Consider the two rasters R_1 and R_2 in Figure 4.12. (b). They are not being pulled apart but are being stretched as the tensile load on the bottom surface of the coupons is acting along the length of the rasters. This results in higher apparent yield strength in comparison to the strength associated with breaking the LCA bonds in horizontal build. Thus, the difference in location of contours and FDM fabrication result in the vertical build displaying better mechanical properties in comparison to the horizontal build. The gradual deterioration of the bottom surface comprising of contours for different strain values ranging from 3% to 5% is shown in Figure 4.13.

During the 3-point bend test, the tension in the bottom surface of flexural coupons increased continuously as the loading increased until the strain reached a standard 5% strain. The surface remains intact until 3% strain and does not display any signs of stress whitening as shown in Figure 4.13. (A). As the strain in the coupon increases to 3.5%, the rasters begin stretch as shown in Figure 4.13. (B). This stretching of rasters keeps on increasing with increase in strain value to 4% as shown in Figures 4.13. (C) and to 5% as shown in Figure 4.13. (D) and eventually leads to the failure of the flexural coupons. It is evident that a larger force is required for a coupon to fail if the tensile force is acting along the length of the rasters as opposed to acting at an angle to the raster (*in the case of horizontal build*). Thus, the stretching of raster in the bottom surface due to the tensile stress in the case of vertical build is the main reason behind the higher mechanical properties of vertical build coupons in comparison to horizontal build coupons.

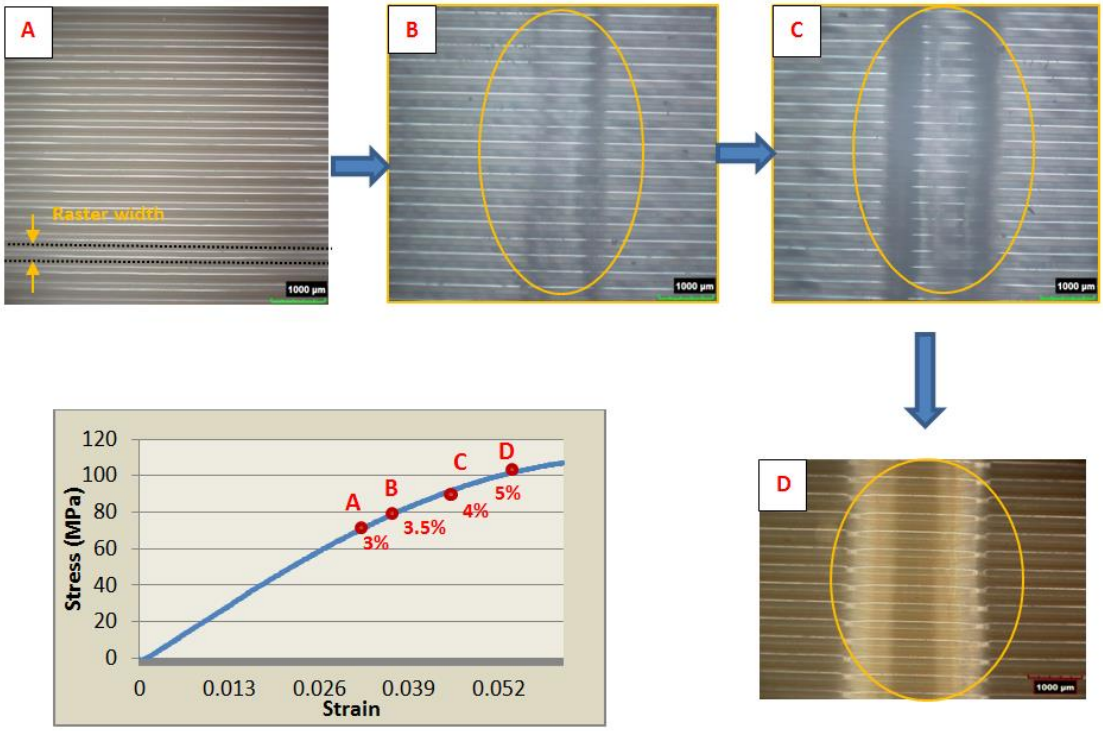

Figure 4.13. Deterioration of the bottom surface of vertical build flexural coupons with increase in strain

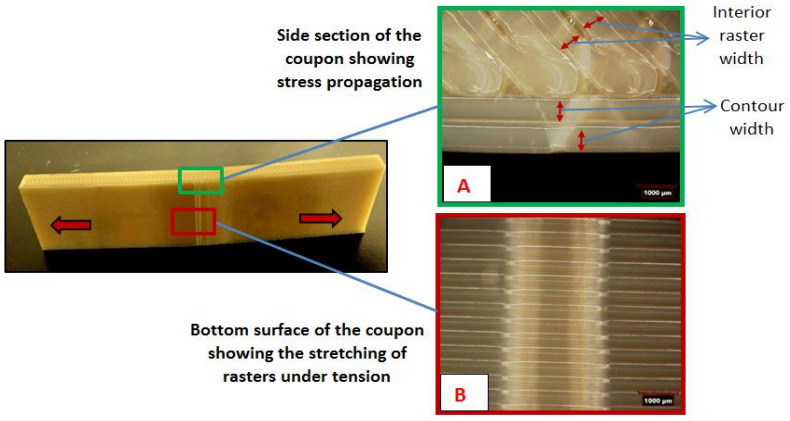

Figure 4.14. Coupon showing the deformed surface and stress whitening after loading at 5% strain

Shown in Figure 4.14. are the deformed surfaces of the loaded test coupons of vertical build. Figure 4.14. (A) shows the stress propagation on the side section towards

the upper surface of the flexural coupon at 5% strain. Figure 4.14. (B) shows rasters that are stretched out in the bottom surface of a flexural coupon at 5% strain. As mentioned earlier, the top and bottom surfaces of the flexural coupon comprise of contours and are under compression (on top) and tension (on bottom).

4.3.2 Compression Test. In the previous studies conducted by Bagsik *et al.* [2], a qualitative reasoning for the behavior of compression coupons has been discussed. According to the study conducted, the compression coupons built in vertical direction fail under compressive load due to the buckling of layers as shown in Figure 4.15. (a), whereas the coupons built in horizontal direction fail under a higher compressive load due to inter-layer sliding as shown in Figure 4.15. (b). Hence, the horizontally built coupons have better mechanical properties in comparison to vertically built coupons.

The buckling of vertical built coupons observed by Bagsik *et al.* agree with our experimental observations (*which will be discussed in Section 6*). However, we did not observe the inter-layer sliding shown in Figure 4.15. (b) in our testing as the testing was conducted only till the coupon underwent 10% deflection. Further explanation of compression coupons is provided in Section 6.

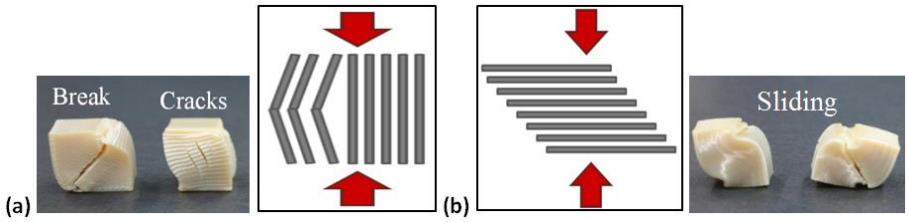

Figure 4.15. Failure of compression specimens built in (a) Vertical direction; (b) Horizontal direction from Bagsik *et al*. [2]

5. EXPERIMENTAL INVESTIGATION OF VARIATION IN BUILD PARAMETERS

As stated before, the first set of experiments (*presented in Section 3*) deal with only the understanding of the effect of build direction on mechanical properties of FDM fabricated coupons under three different temperatures. Using the observations from that study, a qualitative reasoning was presented (*in Section 4*) to comprehend the behavior of test coupons for horizontal and vertical build directions. In this section, an experiment was designed to conduct flexural and compression tests with the build parameters under investigation including build direction, raster angle and negative air gap and to perform a statistical evaluation of the obtained data. The individual effects of these parameters and interaction between these parameters were studied using a full-factorial design of experiment. The testing was carried out for two build styles, sparse and solid. Shown below are the experimental designs for each experiment and the build parameters under consideration depending on the build styles.

Factors and Levels: The flexural and compression tests were done in accordance to the testing standards. The factors under consideration for solid build are build direction, raster angle and air gap. In the case of sparse build, the air gap is kept constant at 2.54 mm (0.1”) and the only factors under consideration are build direction and raster angle as shown in Table 5.1.

Table 5.1. Factors under consideration for flexural test

For solid build style	For sparse build style
Build Direction	Build Direction
Raster Angle	Raster Angle
Air Gap	-

In an experimental design, the independent variables are known as ‘factors’ and different variations of these independent variables are known as ‘levels’. In the case of solid build style, there are three factors as given in the Table 5.1. and each of these

factors has a number of levels. Build direction has 2 levels (horizontal and vertical), raster angle has two levels [(0°, 90°) and (45°, -45°)] and air gap has three levels [-0.00635 mm (-0.00025”), -0.0127 mm (-0.0005”) and -0.01905 mm (-0.00075”)]. Increase in the magnitude of negative air gap will generally increase the overall strength of the coupon, but as the negative air gap increases after a certain limit, the surface quality of the fabricated coupon begins to deteriorate. In this study, the machine used (Fortus 400 mc) had a capability of printing good quality parts until a negative air gap of -0.01905 mm. Hence, the three chosen air gaps were selected at equal intervals between zero and the maximum negative air gap possible.

The test coupons take on all possible combinations of these levels across all the factors. In this case, there are 12 combinations in total and each combination is replicated 5 times resulting in a total of 60 observations. The different levels for each of the factors taken into consideration are shown in Table 5.2.

Table 5.2. Level settings for solid build style

Factors	Levels		
	-1	0	1
Build direction	Horizontal	-	Vertical
Raster angle (degree)	0-90	-	45-45
Air Gap (mm)	-0.00635	-0.0127	-0.01905

Similarly, the level settings for sparse build style are shown in Table 5.3.

Table 5.3. Level settings for sparse build style

Factors	Levels		
	-1	0	1
Build direction	Horizontal	-	Vertical
Raster angle (degree)	0-90	-	45-45

In the case of sparse build styles, there are only two factors under consideration as the third factor, air gap, is fixed at 2.54 mm (0.1”). Build direction has two levels (horizontal and vertical) and raster angle has two levels [(0°, 90°) and (45°, -45°)]. There are 4 different combinations of these levels and each combination is replicated 5 times resulting in a total of 20 observations for sparse build coupons.

6. EXPERIMENTAL RESULTS AND DISCUSSION

6.1 FLEXURAL TESTING – SOLID BUILD STYLE

Flexural testing was conducted according to the previously used standards, i.e., a 3 point bend test conducted according to ASTM D790 standard at a loading rate of 2.56 mm/min (0.1 in/min). The dimensions of the coupons remain the same as before (i.e. 127 mm x 25.4 mm x 6.35 mm).

A total of 60 specimens were tested for 12 different combinations of solid build parameters. The response variables (dependent variables) under observation are yield strength, flexural modulus, strength/weight ratio and modulus/weight ratio. The averaged values of the various mechanical properties are shown in Table 6.1. The detailed dataset obtained for calculating the averages is given in Appendix C.

Table 6.1. Mechanical properties of solid build styles for flexural testing. (H: Horizontal build; V: Vertical build; 0: (0º, 90º); 45: (45º, -45º); 1: Air gap= -0.00635 mm; 2: Air gap= -0.0127 mm; 3: Air gap= -0.01905 mm)

Pattern	Build	Raster	Air Gap (mm)	Build Time (Min)	Strength (MPa)	Mass (g)	Modulus (MPa)	Strength /Mass Ratio (MPa/g)	Modulus /Mass Ratio (MPa/g)
H-0-1	H	0-90	-0.00635	27	69.8	23.53	2005	2.97	85.21
H-0-2	H	0-90	-0.0127	27	75.6	23.85	2110	3.17	88.47
H-0-3	H	0-90	-0.01905	28	81.1	23.95	2241	3.39	93.57
H-45-1	H	45-45	-0.00635	29	66.5	23.81	1890	2.79	79.38
H-45-2	H	45-45	-0.0127	29	69.6	24.06	1963	2.89	81.59
H-45-3	H	45-45	-0.01905	29	76.3	24.31	2052	3.14	84.41
V-0-1	V	0-90	-0.00635	33	91.3	21.35	2491	4.28	116.67
V-0-2	V	0-90	-0.0127	33	92.5	21.44	2511	4.31	117.12
V-0-3	V	0-90	-0.01905	34	93.6	21.53	2560	4.35	118.9
V-45-1	V	45-45	-0.00635	38	86.7	22.19	2351	3.91	105.95
V-45-2	V	45-45	-0.0127	38	87.8	22.4	2368	3.92	105.71
V-45-3	V	45-45	-0.01905	39	88.1	22.6	2395	3.9	105.97

A graphical representation of the data in Table 6.1. along with standard deviations is shown below in Figure 6.1.

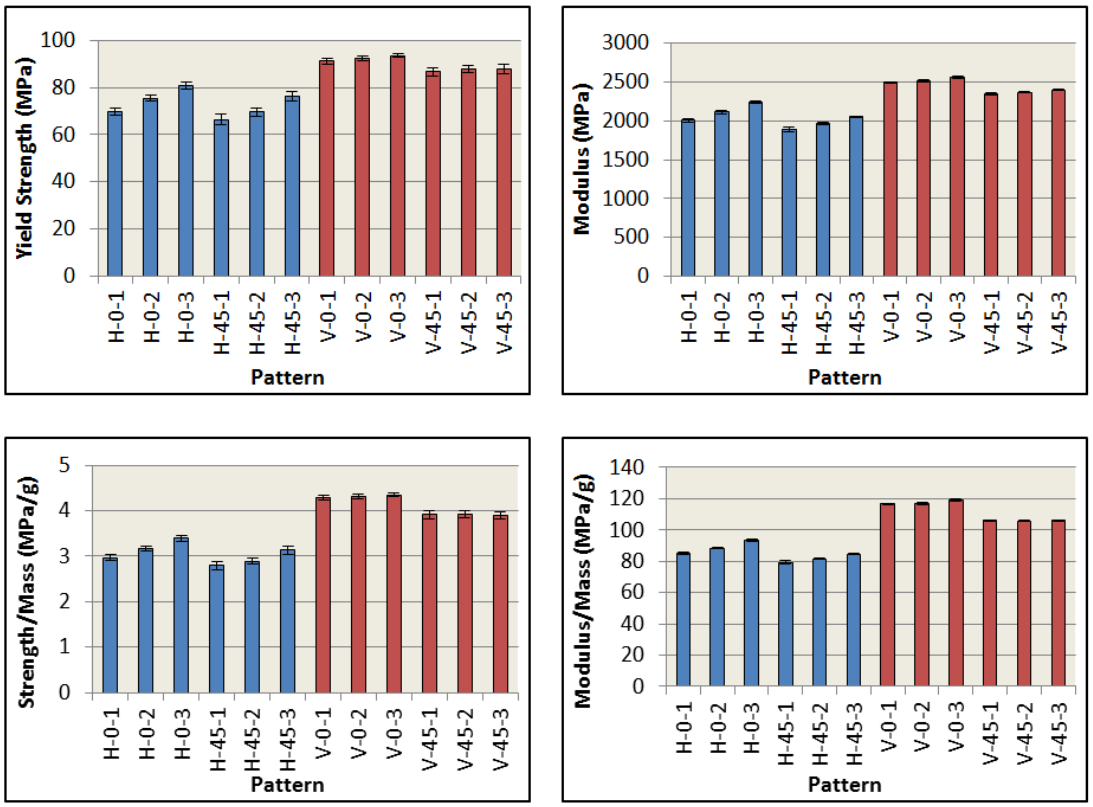

Figure 6.1. Comparison of mechanical properties for solid coupons from flexural testing

6.1.1 Main Effects and Interactions. A full factorial statistical experiment was carried out on the results obtained to determine the main effects and interactions between the parameters used. Main effect is defined as the effect of an independent variable on a response variable averaging across different levels of other independent variables. If the effect of one independent variable on the response variable is dependent on the value of another independent variable then those two variables are said to exhibit interaction. The independent variables in this case are build direction, raster angle and air gap. The response variable considered for the statistical experiment is yield strength. Statistical analysis software JMP 11 was used for the determination of main effects and interactions.

The effects table and interaction plot in Table 6.2. and Figure 6.2., respectively, shows the P-values for main effects and interactions between the factors. The P-value [19] defines the level of significance within a statistical test. It represents the probability of a factor affecting the outcome (response variable).

Table 6.2. Effects table for different solid build factors in flexural tests

Factor	Sum of Squares	F Ratio	P- Value
Build direction	4893.9	4081.07	**<.0001**
Raster angle	360.9	300.96	**<.0001**
Air gap	371.29	309.62	**<.0001**
Build*Raster	4.2	3.5	0.0656
Build*Air gap	306.53	255.62	**<.0001**
Raster*Air gap	4.02	3.35	0.0715

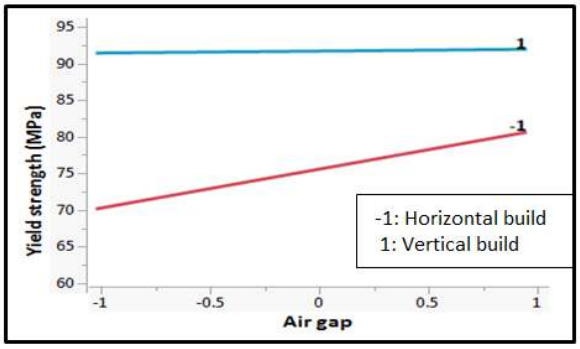

Figure 6.2. Interaction plot for build direction and air gap

According to the statistical experiment, if P-value is less than 0.05 (i.e. for a significance level of higher than 95%) the corresponding factor has a significant effect on the response variable. In Table 6.2., P-values less than 0.05 are highlighted. In this case, it reveals that all of the parameters including build direction, raster angle and air gap have main effects on the response variable, yield strength. Also, the effects table indicates an interaction between build direction and air gap, which means that the effect of air gap on the response variable is dependent on build direction. This interaction can be seen in the plot shown in Figure 6.2. where the blue line represents the vertical build direction and the red line represents the horizontal build direction. In the case of horizontal build, as the magnitude of negative air gap increases, the yield strength also increases. But, in the case of vertical build, the effect of air gap on yield strength is not statistically significant.

6.1.2 Effects of Individual Build Parameters. The main effect of individual variables considered during the statistical experiment is shown below.

6.1.2.1 Effect of build direction. From Figure 6.1. it can be seen that the strength of coupons built in vertical direction is 15% to 30% higher for solid build styles. According to the effects table in Table 6.2., this difference is statistically significant as P-value < 0.05. This is expected as the tension on the bottom surface acts along the length of the contour lines in the case of vertical coupons, thus providing higher resistance to the applied load in comparison to the horizontal build coupons.

6.1.2.2 Effect of raster angle. The effect of raster angle on horizontal and vertical build coupons is graphically shown in Figures 6.3. and 6.4.

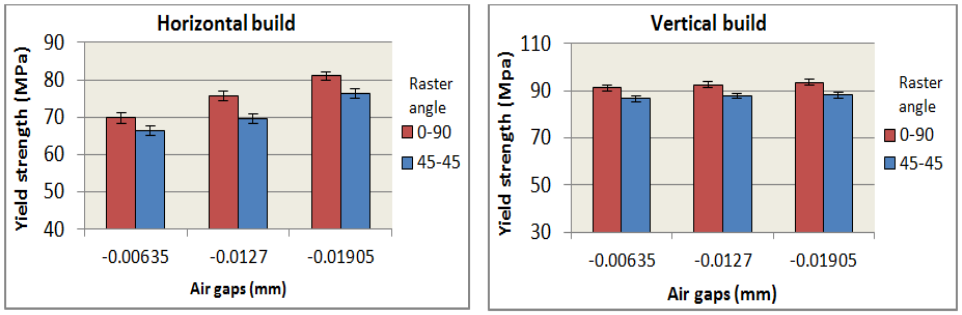

Figure 6.3. Effect of raster angle on yield strength of horizontal and vertical solid coupons from flexural testing

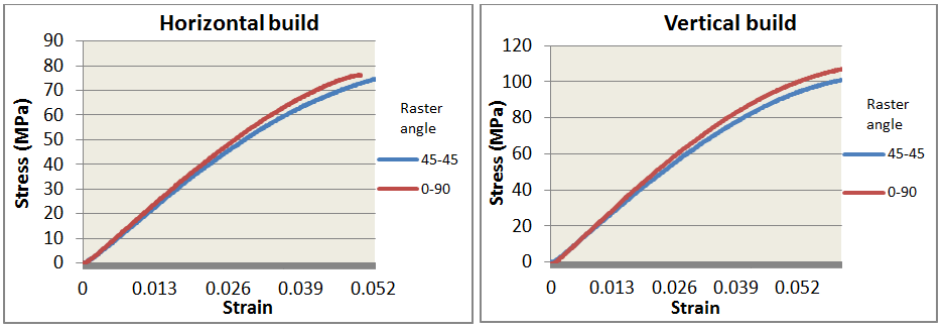

Figure 6.4. Sample stress-strain graphs for horizontal and vertical flexural solid coupons built with an air gap of -0.00635mm

Horizontal build: According to the graphs in Figures 6.3. and 6.4., the horizontal build coupons with (0°, 90°) raster angles have higher yield strength in comparison to the ones with (45°, -45°) raster angles. The trend remains the same for different values of air

gap. According to the experimental investigation presented in Section 3, this happens because in the case of (0°, 90°) raster angles, the rasters in the bottom surface of the coupon are at an angle of 0 degrees to the horizontal axis. This means that the tension experienced in the bottom surface of the coupons is along the length of the rasters.

Vertical build: From the graphs in Figures 6.3. and 6.4., the vertical coupons with (0°, 90°) raster angles exhibit higher yield strength in comparison to the coupons with (45°, -45°) raster angles. The trend remains the same for different air gaps. Similar to the horizontal build, the tensile load acting on the (0°, 90°) rasters in the case of vertical build is along the length of the raster, thus resulting in higher yield strength when compared to (45°, -45°) raster angles.

Irrespective of the build direction, for both solid and sparse build style, coupons with (0°, 90°) raster angle exhibit 5-10% higher flexural strength in comparison to the ones with (45°, -45°) raster angle.

6.1.2.3 Effect of air gap. The effect of raster angle on horizontal and vertical build coupons is graphically shown in Figures 6.5. and 6.6.

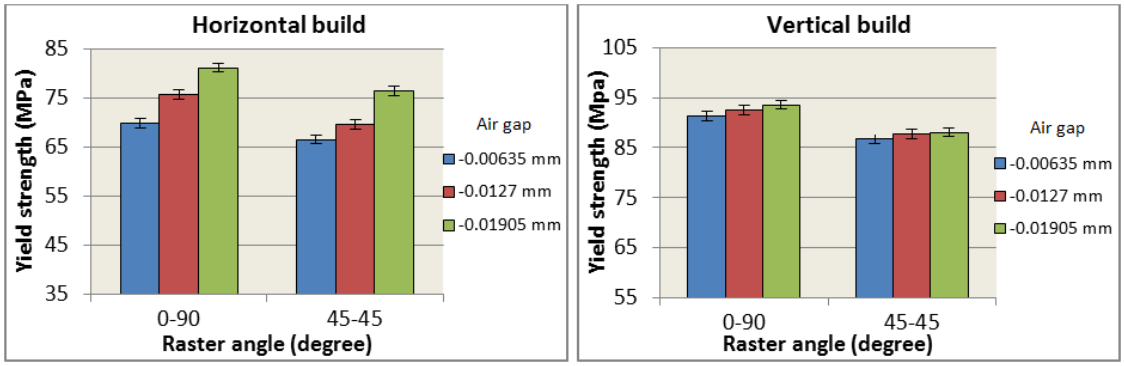

Figure 6.5. Effect of air gap on yield strengths of solid horizontal and vertical coupons from flexural testing of solid coupons

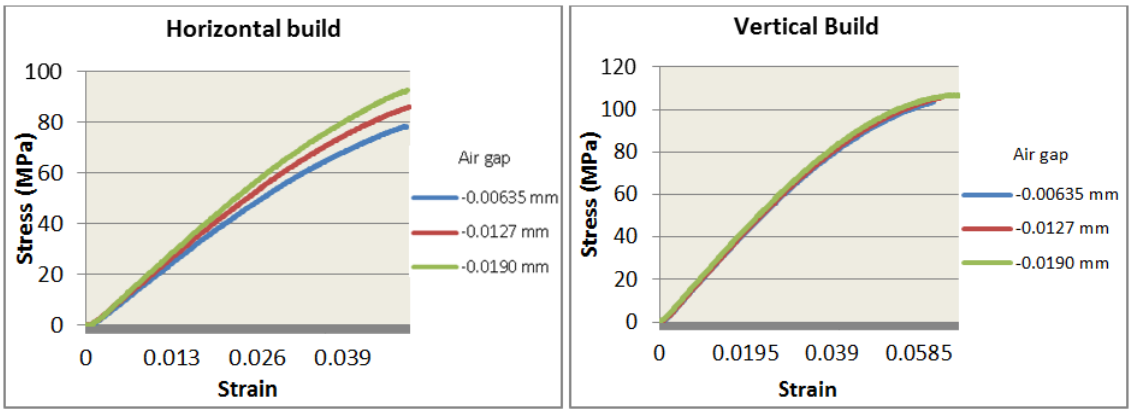

Figure 6.6. Sample stress-strain graphs for horizontal and vertical flexural coupons built with (0, 90) raster angle

Horizontal build: From the above graphs, it can be seen that the yield strength of horizontal build coupons increases with increase in the magnitude of negative air gap. The trend remains the same for different raster angles [(0°, 90°) and (45°, -45°)]. The flexural yield strength increases by 5-10% with increase in the magnitude of negative air gap. According to the experimental investigation, in the case of horizontal build coupons, the increase in the magnitude of negative air gap would help strengthen the LCA bond between the rasters. However, as stated earlier in Section 5, it should be noted that although the increase in the magnitude of negative air gap will generally increase the overall strength of the coupon, as the negative air gap increases after a certain value (-0.01905 mm in this case), the surface quality of the fabricated coupon begins to deteriorate and may also damage the machine.

Vertical build: From the above comparison and interaction plots in Figure 6.2., it can be seen that the effect of air gap in vertical build is not as significant as in the case of horizontal build. With increasing magnitude of negative air gap, the yield strength tends to remain approximately constant. The slight increment of strength across different air gaps can be due to the little increment in the total material volume (because of negative air gaps). The trend remains the same for both raster angles [(0°, 90°) and (45°, -45°)]. This can be expected because in the case of vertical build flexural coupons, the air gaps between the rasters do not offer any resistance to the applied load. The resistance in vertical build coupons is offered by the rasters in the bottom surface and the HCA bonds

between the layers. From the above comparison and statistical data given in Table 6.2., it can be concluded with that the effect of air gap on vertical build coupons is not significant (P-value>0.05).

Inducing negative raster air gaps can improve the mechanical properties of the coupons built in horizontal build direction as the LCA bonds have a direct impact in this build direction. Figure 6.7. shows the microscope images of different air gaps used in FDM. The increment in the volume of material due to negative air gap is neglected as the change is very small (< 1%).

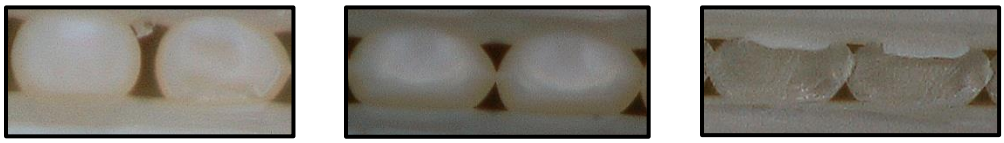

Positive air gap Zero air gap Negative air gap

Figure 6.7. Different air gaps in solid build style

6.2 FLEXURAL TESTING – SPARSE BUILD STYLE

The independent variables/factors under consideration in sparse build style are raster angles and build direction. The air gap used for sparse build coupons was 2.54 mm (0.1”). A total of 20 specimens were tested for 4 different combinations and 5 replications. The averages values of these combinations are shown in Table 6.3. The detailed dataset obtained for calculating the averages is given in Appendix D.

Table 6.3. Mechanical properties of sparse build style with different build directions. (S-H: Sparse horizontal; S-V Sparse vertical; 0: Raster angle= (0, 90); 1: Raster angle= (45, -45))

Pattern	Build	Raster	Time (min)	Strength (MPa)	Mass (g)	Modulus (MPa)	Strength/ Mass	Modulus/ Mass
SH-0	H	0-90	22	66.3	18.26	1870	3.63	102.41
SH-45	H	45-45	23	58.5	18.67	1768	3.13	94.7
SV-0	V	0-90	28	75.4	17.44	2070	4.32	118.69
SV-45	V	45-45	31	65.8	18.38	1860	3.58	97.48

6.2.1 Main Effects and Interactions. A full factorial experiment was conducted to determine the statistical significance of the parameters used. The individual parameters in this case were build direction and raster angle. The effects table in Table 6.4. shows the main effects and interaction between the parameters used.

Table 6.4. Effects table for different sparse build factors in flexure tests

Factor	Sum of Squares	F Ratio	P- Value
Build direction	332.92	158.34	<.0001
Raster angle	374.97	178.35	<.0001
Build*Raster	4.23	2.01	0.1752

From the P-values in Table 6.4, it can be inferred that the individual parameters build direction and raster angle each have a significant effect (P-value < 0.05) on the response variable of the experiment i.e. yield strength. There is no significant interaction between the two parameters which means that the effect of each parameter is independent of the other.

6.2.2 Effects of Individual Build Parameters. The main effect of individual variables considered during the statistical experiment is shown below.

6.2.2.1 Effect of build direction. The effect of build direction on the flexural yield strength on solid and sparse build style coupons is shown graphically in Figure 6.8.

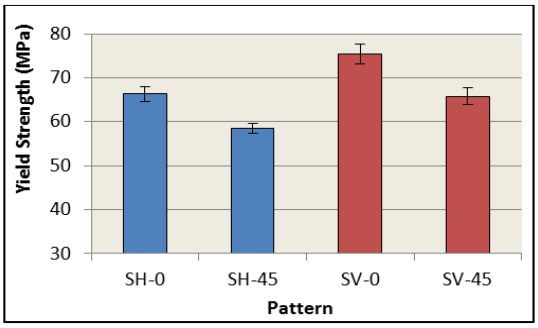

Figure 6.8. Effect of build direction for horizontal and vertical build sparse coupons from flexural testing

From Figure 6.8., it is evident that the strength of coupons built in vertical direction is about 15% higher than horizontal direction for sparse build styles. According to the effects table in Table 6.4., this difference is statistically significant. As stated earlier in Section 4, this behavior is expected as the tension on the bottom surface acts along the length of the contour lines in the case of vertical coupons, thus providing higher resistance to the applied load in comparison to the horizontal build coupons.

6.2.2.2 Effect of raster angle. The effect of raster angle on the flexural yield strength on horizontal and vertical build style coupons is shown graphically in Figures 6.9. and 6.10.

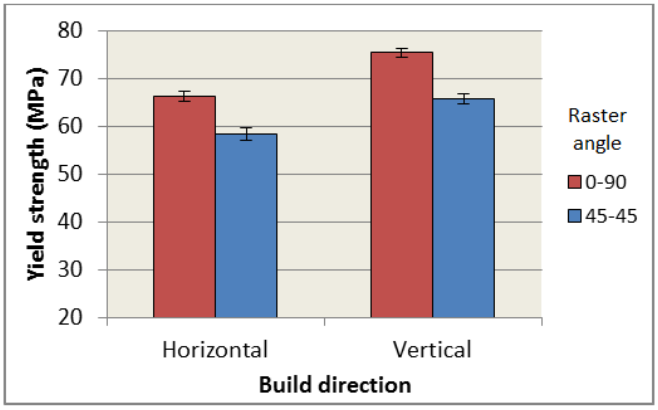

Figure 6.9. Effect of raster angle for horizontal and vertical build sparse coupons from flexural testing

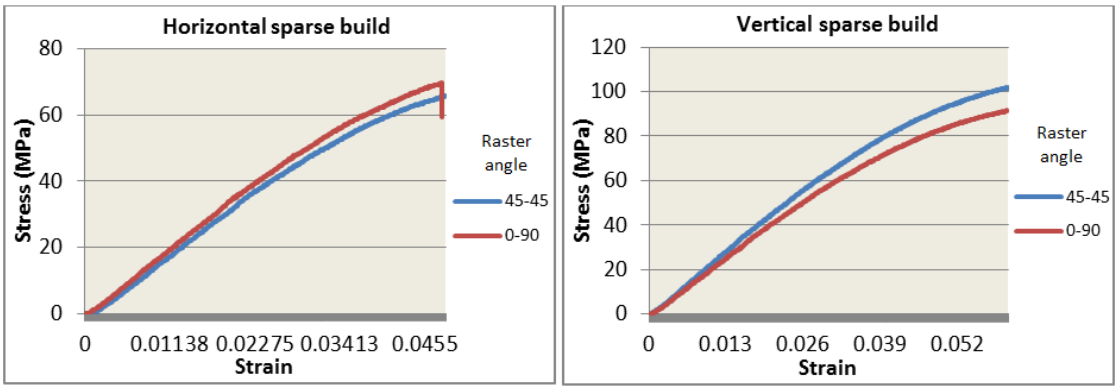

Figure 6.10. Sample stress-strain graphs for horizontal and vertical built sparse flexural coupons

According to the Figures 6.9. and 6.10., in both horizontal and vertical specimens, the coupons with (0°, 90°) raster angle have relatively higher strength in comparison to the coupons with (45°, -45°) raster angle. This is expected as the load acts along the length of the rasters in the case of (0°, 90°) raster angle and offers higher resistance to the applied load in comparison to the (45°,45°) raster angle coupons.

6.3 COMPRESSION TESTING – SOLID BUILD STYLE

Compression testing was conducted according to the standards used in Section 3. The loading rate of 1.27 mm/min (0.05 in/min) was used. The dimensions of the coupons remain the same as before (i.e. 38.1 mm x 38.1 mm x 25.4 mm). A total of 60 coupons were tested for 12 different combinations for solid build. The response variables (dependent variables) under observation are yield strength, flexural modulus, strength/weight ratio and modulus/weight ratio. The averaged values of mechanical properties are given in Table 6.5. The detailed dataset obtained for calculating the averages is given in Appendix E.

Table 6.5. Mechanical properties of solid build styles for flexural testing. (CH: Horizontal build; CV: Vertical build; 0: (0º, 90º) angle; 45: (45º, -45º) angle; 1: Air gap= -0.00635 mm; 2: Air gap= -0.0127 mm; 3: Air gap= -0.01905 mm)

Pattern	Build	Raster	Air Gap (mm)	Time (min)	Mass (g)	Strength (MPa)	Modulus (MPa)	Strength/ mass (MPa/g)	Modulus /mass (MPa/g)
CH-0-1	H	0-90	-0.00635	43	40.28	85.4	885	2.12	21.97
CH-0-2	H	0-90	-0.0127	44	4077	86.3	892	0.02	0.22
CH-0-3	H	0-90	-0.01905	44	41.26	86.5	898	2.1	21.76
CH-45-1	H	45-45	-0.00635	46	40.89	85.8	884	2.1	21.62
CH-45-2	H	45-45	-0.0127	46	41.34	85.9	896	2.08	21.67
CH-45-3	H	45-45	-0.01905	47	41.81	86.4	893	2.07	21.36
CV-0-1	V	0-90	-0.00635	45	40.17	72.8	821	1.81	20.44
CV-0-2	V	0-90	-0.0127	46	40.55	73.1	819	1.8	20.2
CV-0-3	V	0-90	-0.01905	46	40.77	73.6	820	1.81	20.11
CV-45-1	V	45-45	-0.00635	48	40.6	65.3	744	1.61	18.33
CV-45-2	V	45-45	-0.0127	49	40.98	65.8	746	1.61	18.2
CV-45-3	V	45-45	-0.01905	49	41.45	66.1	754	1.59	18.19

A graphical representation of data in Table 6.5. along with standard deviation is shown in Figure 6.11.

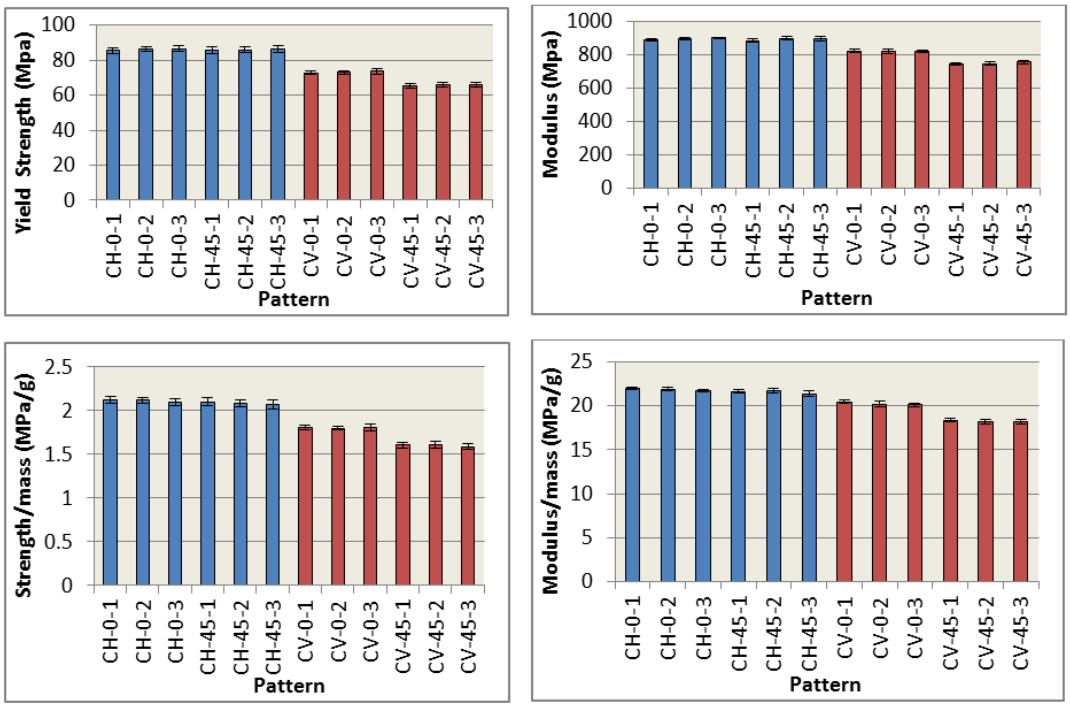

Figure 6.11. Comparison of mechanical properties for solid coupons from compression testing.

6.3.1 Main Effects and Interactions. Similar to the flexural experiment, a full factorial statistical experiment was carried out on the results obtained to determine the main effects and interactions between the parameters used. The independent variables in this case are build direction, raster angle and air gap. The response variable considered for the statistical experiment is yield strength. Statistical analysis software JMP 11 was used for the determination of main effects and interactions. The effects table and interaction plots are shown in Table 6.6. and Figure 6.12., respectively.

Table 6.6. Effects table for different solid build factors in compression tests

Factors	Sum of Squares	F Ratio	P-value
Build direction	4775.5037	8392.691	<.0001
Raster angle	343.6323	603.9153	<.0001
Air gap	6.9546	3.4946	0.0816
Build*Raster	249.6281	438.708	<.0001
Build*Air gap	1.5674	2.7547	0.1019
Raster*Air gap	0.7047	1.2385	0.2699

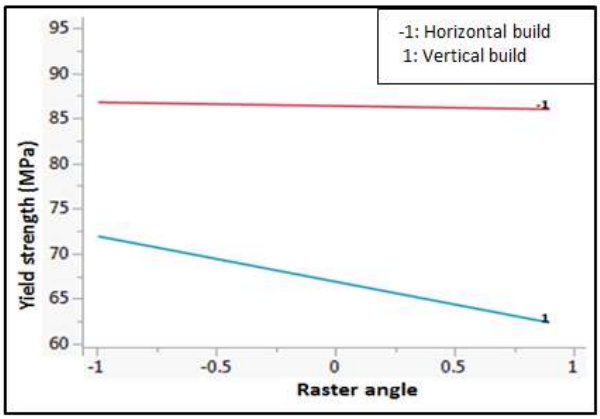

Figure 6.12. Build vs. raster interaction plot

From the P-values in Table 6.6., it can be seen that the parameters build direction and raster angles have main effects on the final response variable, yield strength. Also, the effect table indicates an interaction between build direction and raster angle, which means that the effect of raster angle is dependent on build direction. This interaction can be seen in the plot shown in Figure 6.12. where the blue line represents the vertical build direction and the red line represents the horizontal build direction. For the vertical build coupons, (0°, 90°) raster is better than (45°, -45°) since its yield strength is higher. But for the horizontal build coupons, P-value > 0.05 (from Table 6.6) indicates that the effect of raster angle is not statistically significant.

6.3.2 Effects of Individual Build Parameters. The main effect of individual variables considered during the statistical experiment is shown below.

6.3.2.1 Effect of build direction. From Figure 6.11., it can be seen that the strength of coupons built in horizontal direction is 15% to 24% higher than that in vertical direction for solid build styles. This is expected as the tension on the bottom surface acts along the length of the contours in the case of vertical coupons and provides higher resistance to the applied load in comparison to the horizontal build coupons.

6.3.2.2 Effect of raster angle. The effect of raster angle on the horizontal and vertical build coupons is studied using the graphs and plots in Figures 6.13. and 6.14.

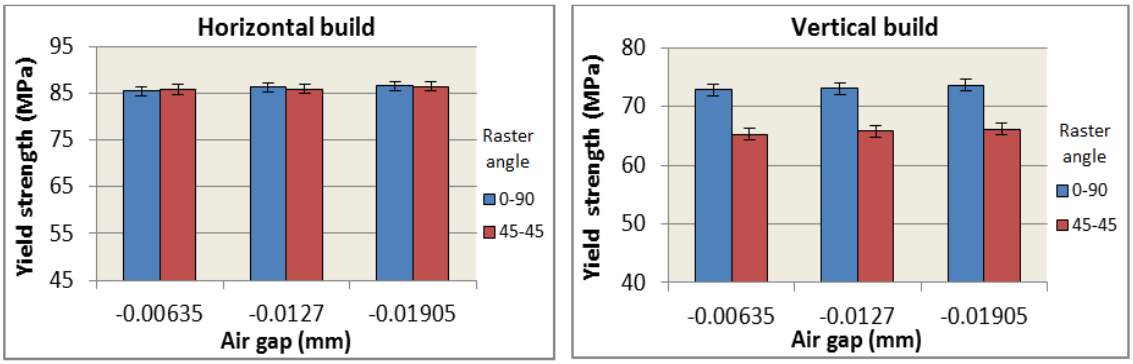

Figure 6.13. Effect of raster angle on the yield strengths of horizontal and vertical build solid coupons from compression testing

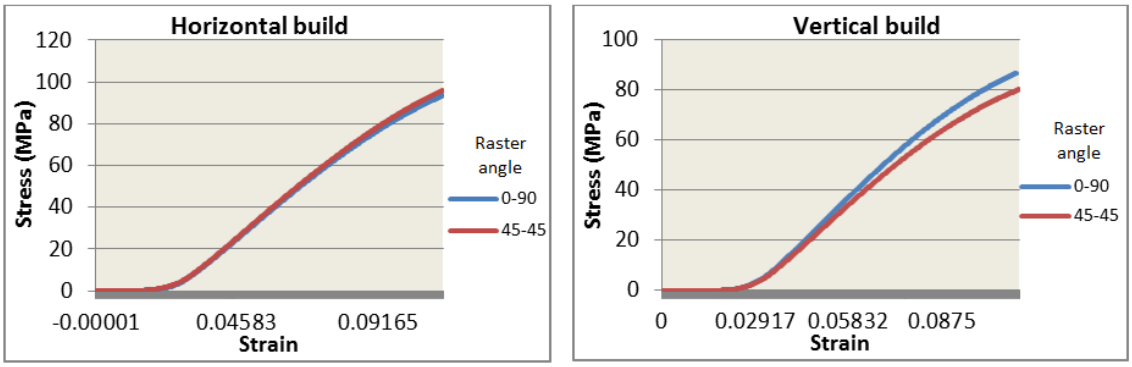

Figure 6.14. Sample stress-strain graphs for horizontal and vertical compression solid coupons built with an air gap of -0.00635mm

Horizontal build: From the above comparison and the effects table in Table 6.6., it can be seen that in the case of horizontal coupons, the effect of raster angle on yield strength is not significant (P-value >0.05). This is expected as the load applied on the coupon acts perpendicular to the layer in which the rasters are present, thus the strength of horizontal coupons is independent of the raster angle; refer to Figure 6.15.

Vertical build: In the case of vertical solid coupons, the coupons with (0°, 90°) raster angle have about 12% higher yield strength in comparison to the coupons with (45°, -45°) raster angle. According to the data in Table 6.6., this difference is statistically significant with a P-value < 0.05. This indicates that the deposited lines in the (0°, 90°) angle act as stiffeners to the structures and offering more resistance to deformation (*further discussion in Section 6.5)*; refer to Figure 6.16.

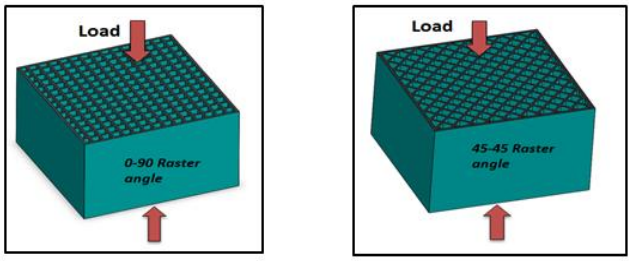

Figure 6.15. Physical models for horizontal built compression solid coupons with (0°, 90°) and (45°, -45°) raster angles

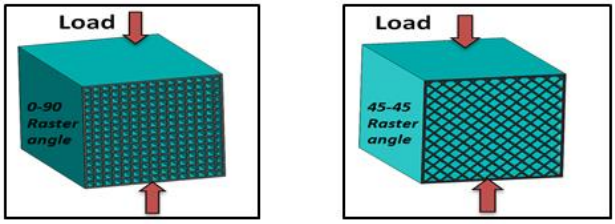

Figure 6.16. Physical models for horizontal built compression coupons with (0°, 90°) and (45°, -45°) raster angles

6.3.2.3 Effect of air gap. The effect of air gap on the horizontal and vertical coupons is studied using the graphs and plots in Figures 6.17. and 6.18.

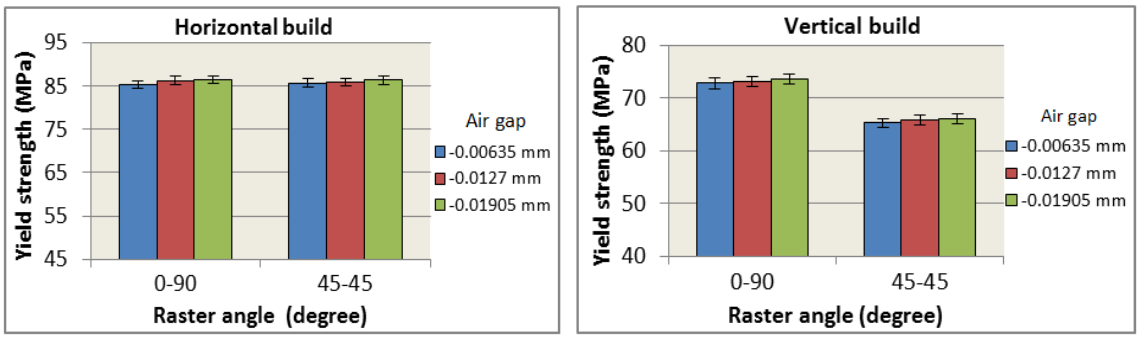

Figure 6.17. Effect of air gap on yield strengths of horizontal and vertical build solid coupons from compression testing

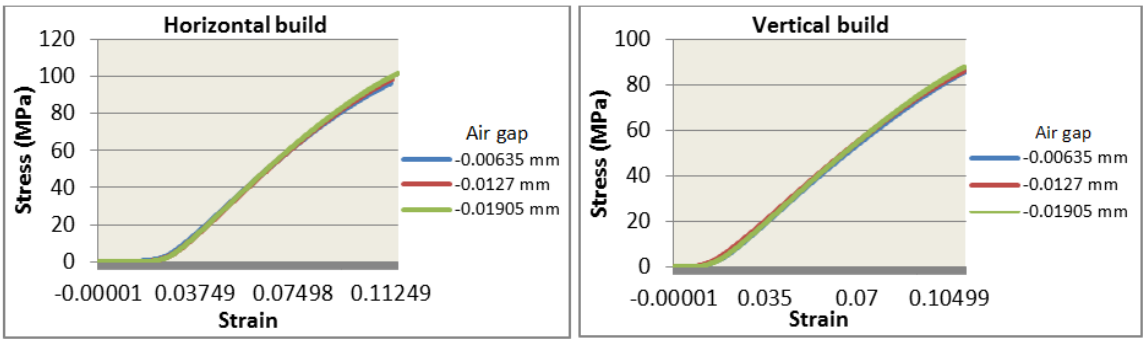

Figure 6.18. Sample stress-strain graphs for horizontal and vertical built solid flexural coupons with (0º, 90º) raster angle

Horizontal build: From the above two figures and the effects table in Table 6.6, it can be seen that in the case of horizontal build coupons, the effect of air gap is not significant with a P-value > 0.05. The trend remains the same for (0°, 90°) and (45°, -45°) raster angles. This is because in the case of horizonatal build, the coupons fail due to inter-layer sliding [5]. The variation in air-gap between the rasters does not have a significant effect on the overall sliding failure, thus the strength of horizontal build coupon is statistically independent of air gap.

Vertical build: Similar to horizontal build, the effect of air gap in vertical build is also not significant (Table 6.6.) and the trend remains the same for (0°, 90°) and (45°, -45°) raster angles. As indicated by the effects table, there is no main effect of air gap for either horizontal build or vertical build.

6.4 COMPRESSION TESTING – SPARSE BUILD STYLE

The sparse build coupons were tested at a loading rate of 1.27 mm/min (0.05 in/min). The independent factors under consideration in sparse build style were raster angle and build direction. The air gap used was 2.56 mm (0.1”). A total of 20 specimens were tested for 4 different combinations and 5 replications. The average values of each run are shown in Table 6.7. The detailed dataset obtained for calculating the averages is given in Appendix F.

Table 6.7. Compression- Mechanical properties of sparse build style with different build directions. (CSH: Sparse horizontal; S-V Sparse vertical; 0: Raster angle= (0º, 90º); 45: Raster angle= (45º, -45º))

Run	Build	Raster	Time (min)	Strength (MPa)	Mass (g)	Modulus (MPa)	Strength /Mass (Mpa/g)	Modulus/ Mass (Mpa/g)
CSH-0	H	0-90	28	45.6	23.61	642	1.92	27.19
CSH-45	H	45-45	32	46.2	24.7	649	1.87	26.28
CSV-0	V	0-90	35	36.9	23.38	543	1.49	23.22
CSV-45	V	45-45	38	25.8	24.68	450	1.05	18.23

6.4.1 Main Effects and Interactions. A full factorial statistical experiment was conducted to determine the main effects and the interactions between the parameters used. The individual parameters used in this experiment were build direction and raster angle. The response variable considered for the statistical experiment was yield strength. Statistical analysis software JMP 11 was used for the determination of main effects and interactions and the results are shown in Table 6.8 and Figure 6.19.

Table 6.8. Effects table of different sparse build factors in compression tests

Factor	Sum of Squares	F Ratio	P- Value
Build direction	1062.88	814.62	<.0001
Raster angle	138.33	106.02	<.0001
Build*Raster	175.23	134.3	<.0001

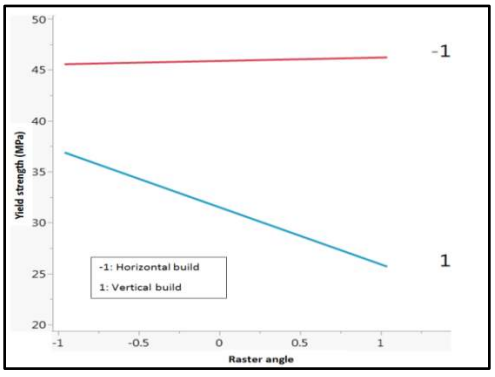

Figure 6.19. Build vs. raster interaction plot

According to the effects table in Table 6.8., a statistically significant interaction exists between build direction and raster angle. This means that the effect of each of these two individual parameters is dependent on the other. This interaction can be clearly seen in the interaction plot shown in Figure 6.19. where the red line represents the horizontal build direction and blue line represents the vertical build direction. The effect of raster angle is statistically significant (P-value < 0.05) only in the case of vertical build coupons, whereas it is not statistically significant for horizontal build coupons.

6.4.2 Effects of Individual Build Parameters. The main effect of individual variables considered during the statistical experiment is shown below.

6.4.2.1 Effect of build direction. Effect of build direction in solid and sparse build coupons is represented graphically in Figure 6.20.

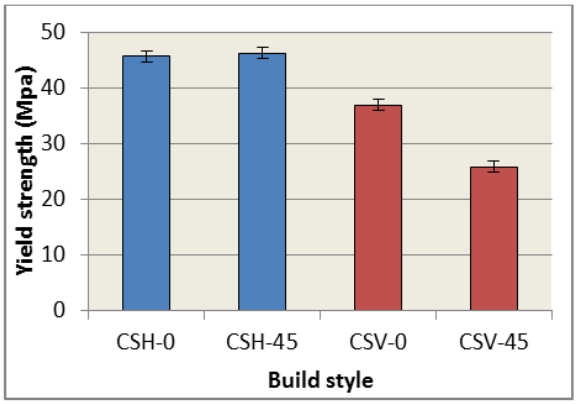

Figure 6.20. Effect of build direction for horizontal and vertical build sparse coupons from compression tests.

In Figure 6.20., red bars represent the coupons fabricated in vertical build direction and blue bars indicate the coupons built in horizontal direction. The strength of coupons built in horizontal direction is 19% to 40% higher than that in vertical direction for sparse build styles. This is expected as the tension on the bottom surface acts along the length of the contours in the case of vertical coupons and provides higher resistance to the applied load in comparison to the horizontal build coupons.

6.4.2.2 Effect of raster angle. Effect of raster angle in horizontal and vertical build coupons is represented graphically in Figures 6.21. and 6.22.

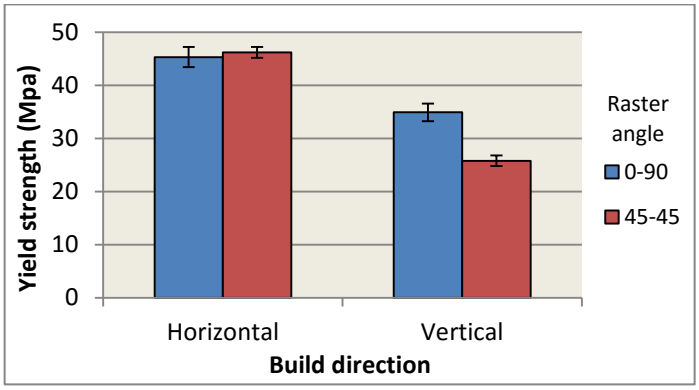

Figure 6.21. Effect of raster angle for horizontal and vertical build sparse coupons in compression tests

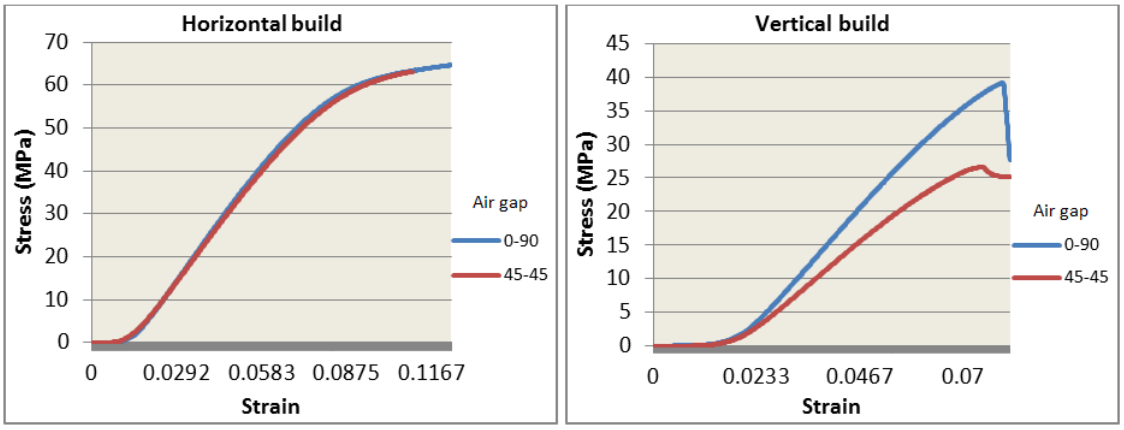

Figure 6.22. Sample stress-strain graphs for horizontal and vertical build sparse coupons in compression tests

Similar to solid build style, the effect of raster angle on horizontal build is statistically not significant (see Table 6.8.). This is expected as the applied compression force acts perpendicular to the layer in which the rasters are present. However, in the case of vertical build, the effect of raster angle is statistically significant (P-value < 0.05) as seen in Table 6.8. and in Figure 6.19. The coupons with (0°, 90°) raster angle have about 30% higher yield strength in comparison to the coupons with (45°, -45°) raster angle.

This indicates that the deposited lines in (0°, 90°) angle act as stiffeners in the case of sparse build styles, thus making (0°, 90°) raster stronger than (45°, -45°) rasters.

6.5 FAILURE OF VERTICAL BUILD SPARSE COUPONS IN COMPRESSION

From the above results, it is evident that the mechanical properties of vertical build sparse compression coupons with (0°, 90°) raster are higher in comparison to the coupons with (45°, -45°) raster angle in compression tests. This is interesting because in the case of (0°, 90°) raster coupons, only the rasters deposited perpendicular to the loading surface will resist the load, whereas in the case of (45°, -45°) rasters, the applied load is taken by all the rasters. This behavior can be better explained by examining the coupons during the compressive testing as shown in Figure 6.23. This figure shows the behavior of coupons during the compression testing for increasing loads. Figure 6.24. represents the load vs. deformation relationship for (0°, 90°) and (45°, -45°) raster coupons. According to the graph, (0°, 90°) coupons exhibit about 40% higher yield strength and stiffness in comparison to (45°, -45°) coupons. In the case of (0°, 90°) raster coupons, the deposited vertical rasters act as struts and resist the deformation until a load of ~43 KN and then the coupon fails all of a sudden internally due to buckling at ~2 mm deformation. In the case of (45°, -45°) raster coupons, the failure does not occur suddenly. The sparse coupon created by (45°, -45°) raster angle has more deformation before failure occurs. The structure reaches a deformation of ~2 mm at a load of ~25 KN which is about 40% less than the failure load of (0°, 90°) raster coupon. All the 5 tested samples for each set of coupons exhibit the same behavior. The failure in the (45°, -45°) raster coupon occurs on the contour of the coupon upon continuous loading as shown in Figure 6.23. Thus, the (0°, 90°) raster coupon is comparatively stiffer and stronger compared to the (45°, -45°) raster coupons.

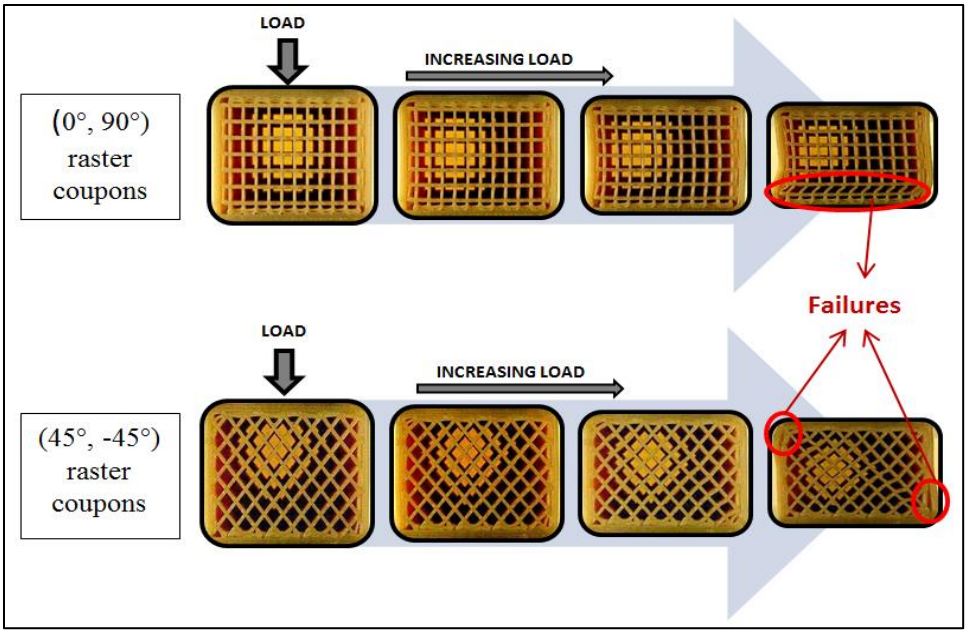

Figure 6.23. Gradual failure of sparse compressive coupons for (0º, 90º) and (45º, -45º) raster angles

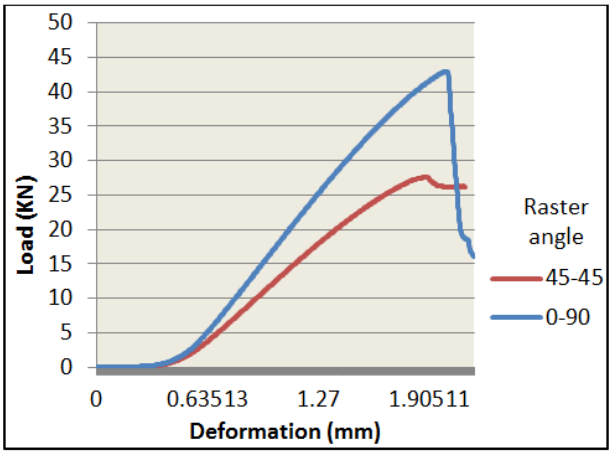

Figure 6.24. Load vs. deformation for sparse build coupons in compression tests

7. CONCLUSION

ULTEM 9085 material was used to fabricate solid and sparse build coupons with variations in build parameters. The mechanical properties of these coupons fabricated by the FDM process using a Fortus 400mc machine were studied. A full factorial statistical experiment was carried out to study the effects of build direction, raster angle and air gap on the flexure and compression properties of the FDM coupons. The experimental investigation included the use of optical images and physical models of the compression and flexural test coupons to comprehend the variations in mechanical properties of the FDM fabricated coupons for different build parameters. The results of this study are summarized below.

- The flexural test results indicate that the vertical build direction exhibits 15-30% higher yield strength in comparison to the horizontal build direction for specimens built with solid and sparse build coupons.
- The compression test results indicate that the horizontal build direction exhibits 15-40% higher compressive strength in comparison to vertical build direction for both solid and sparse build coupons.
- The flexural yield strength of horizontal build solid coupons increases by 5-10% with increase in the magnitude of negative air gap from -0.00635 mm to -0.01905 mm, but the difference is statistically not significant in the case of vertical build coupons.
- For horizontal and vertical build coupons, (0°, 90°) raster angle exhibits 5-10% higher flexural strength for both solid and sparse build coupons in comparison to the (45°, -45°) raster angle.
- The compressive yield strength of vertical build for both solid and sparse coupons increases by 12-30% with (0°, 90°) raster angle in comparison to (45°, -45°) raster angle, but the difference is statistically not significant for horizontal build coupons.

APPENDIX A.

MECHANICAL PROPERTIES OF DIFFERENT BUILD STYLES AT THREE DIFFERENT TEMPERATURES IN FLEXURAL TESTING

Raster width = 0.508 mm (0.02’); Raster angle = (45°, -45°) degrees; Air gap = 0 (solid)

Temperature	Build style	Sample	Yield strength (MPa)	Flexural modulus (MPa)
24 C	S-H	1	65.9	1878
		2	63.71	1893
		3	63.11	1864
		4	64.23	1876
		5	66.54	1862
	SP-H	1	58.4	1806
		2	57.21	1820
		3	55.53	1780
		4	59.4	1781
		5	57.8	1831
	S-V	1	87.83	2386
		2	87.8	2364
		3	84.65	2406
		4	88.4	2373
		5	87.33	2391
	SP-H	1	63.3	1790
		2	62.15	1801
		3	65.21	1830
		4	63.71	1820
		5	64.7	1829

Temperature	Build style	Sample	Yield strength (MPa)	Flexural modulus (MPa)
82 C	S-H	1	41.7	1501
		2	43.21	1472
		3	44.5	1509
		4	43.2	1481
		5	41.7	1487
	SP-H	1	36.16	1323
		2	38.22	1286
		3	35.71	1331
		4	35.88	1316
		5	36.68	1321
	S-V	1	72.44	2080
		2	71.24	2103
		3	70.03	2104
		4	72.93	2116
		5	71.92	2112
	SP-H	1	48.08	1637
		2	47.82	1666
		3	48.16	1643
		4	47.28	1681
		5	47	1664

Temperature	Build style	Sample	Yield strength (MPa)	Flexural modulus (MPa)
121 C	S-H	1	31.18	1330
		2	32.19	1295
		3	32.11	1312
		4	35.72	1323
		5	31.93	1315
	SP-H	1	28.33	1185
		2	29.87	1211
		3	27.7	1207
		4	26.95	1228
		5	29.96	1218
	S-V	1	56.06	1902
		2	57.78	1878
		3	56.66	1919
		4	58.54	1901
		5	57.7	1913
	SP-H	1	46.59	1548
		2	48.03	1563
		3	45.84	1527
		4	46.93	1552
		5	45.91	1524

APPENDIX B.

MECHANICAL PROPERTIES OF DIFFERENT BUILD STYLES AT THREE DIFFERENT TEMPERATURES IN COMPRESSION TESTING

Raster width = 0.508 mm (0.02’); Raster angle = (45°, -45°) degrees; Air gap = 0 (solid)

Temperature	Build style	Sample	Yield strength (MPa)	Compression modulus (MPa)
24 C	S-H	1	84.9	822.3
		2	83.1	841.7
		3	84.3	842.7
		4	86.6	823.9
		5	82.4	836.1
	SP-H	1	45.5	658.2
		2	45.7	637.9
		3	45.3	661.1
		4	47.3	646.1
		5	47	653.4
	S-V	1	62.6	834.5
		2	65.5	805.9
		3	63.8	842.6
		4	62.1	835.6
		5	63.6	819.3
	SP-H	1	27.2	459.1
		2	27.3	460.5
		3	28.9	460.8
		4	28.4	456.1
		5	25.1	446.5

Temperature	Build style	Sample	Yield strength (MPa)	Compression modulus (MPa)
82 C	S-H	1	59.8	801.8
		2	57.6	786.6
		3	59.8	791.7
		4	58.6	795.9
		5	58.1	812
	SP-H	1	35.3	569.3
		2	33.3	569.7
		3	33.7	586.1
		4	34.5	571.7
		5	34.6	578.4
	S-V	1	49.4	750.8
		2	52.4	703.2
		3	51.9	745.3
		4	50.5	743.4
		5	52.5	746.3
	SP-H	1	22.2	388.7
		2	21.5	417.4
		3	22.5	404.8
		4	24.3	426.4
		5	21.5	417.3

Temperature	Build style	Sample	Yield strength (MPa)	Compression modulus (MPa)
121 C	S-H	1	44.9	718.3
		2	46.5	685.5
		3	48.1	653.2
		4	45.1	709.8
		5	46	688.5
	SP-H	1	23.9	489.7
		2	24.8	493.2
		3	23.2	475.8
		4	23.9	498.1
		5	24.3	498.6
	S-V	1	39.8	703.2
		2	40.8	723.9
		3	38.4	689.6
		4	42.6	717.9
		5	39.7	717
	SP-H	1	18.3	410.5
		2	16.8	376.7
		3	16.3	396.8
		4	16.6	409.8
		5	17.8	379.3

APPENDIX C.

MECHANICAL PROPERTIES OF SOLID BUILD COUPONS FOR VARIOUS BUILD PARAMETERS IN FLEXURAL TESTING

Raster width = 0.508 mm (0.02’); Temperature = 24°C

Build	Raster angle	Airgap (mm)	Sample	Yield strength (MPa)	Flexural modulus (MPa)
Horizontal	0-90	-0.00635	1	69.9	1986
			2	69.4	1974.2
			3	70.6	2029.8
			4	70.2	2020.8
			5	68.9	2014.5
	0-90	-0.0127	1	74.3	2083.9
			2	73.5	2116.6
			3	77.1	2115
			4	76.8	2118.7
			5	76.3	2120.3
	0-90	-0.01905	1	82.6	2214.1
			2	81.9	2231.8
			3	80.2	2214.7
			4	80.8	2255.9
			5	80.1	2291.9
	45-45	-0.00635	1	64.8	1869.1
			2	66.7	1868.2
			3	66.3	1931
			4	67.6	1880.2
			5	67.2	1904
	45-45	-0.0127	1	68.5	1977.1
			2	71.6	1950.6
			3	69.8	1972.8
			4	68.5	1967.3
			5	69.6	1948
	45-45	-0.01905	1	77.3	2060.5
			2	78.3	2078.4
			3	76.4	2065.5
			4	75.3	2034.9
			5	74.6	2019.7

Build	Raster angle	Airgap (mm)	Sample	Yield strength (MPa)	Flexural modulus (MPa)
Vertical	0-90	-0.00635	1	91.5	2467.8
			2	90.9	2499.4
			3	91.1	2519.5
			4	92	2470.3
			5	91.1	2493.6
	0-90	-0.0127	1	94.1	2493.9
			2	93	2510.4
			3	90.7	2510.4
			4	93.7	2486
			5	91.3	2460.7
	0-90	-0.01905	1	92.9	2544.5
			2	92.4	2549.3
			3	93.4	2551.1
			4	95.9	2628.4
			5	93.4	2527.4
	45-45	-0.00635	1	87.7	2297.4
			2	86.5	2360.3
			3	84.9	2367.9
			4	87.6	2383.6
			5	86.7	2343.5
	45-45	-0.0127	1	87.1	2358.3
			2	87.3	2378.4
			3	87.3	2382.6
			4	89.4	2373.7
			5	88.3	2350.5
	45-45	-0.01905	1	89.8	2348.3
			2	87.2	2480.9
			3	89.3	2431.8
			4	87	2369.3
			5	87.4	2348

APPENDIX D.

MECHANICAL PROPERTIES OF SPARSE BUILD COUPONS FOR DIFFERENT BUILD DIRECTIONS AND RASTER ANGLES IN FLEXURAL TESTING

Raster width = 0.508 mm (0.02’); Air gap = 2.54 mm (0.1’); Temperature = 24°C

Build	Raster angle	Sample	Yield strength (MPa)	Flexural modulus (MPa)
Horizontal	0-90	1	65.1	1895.9
		2	64.3	1921.2
		3	67.2	1856.2
		4	68.6	1815.8
		5	66.3	1862.7
	45-45	1	59.3	1771.2
		2	58.8	1761.6
		3	59.5	1777.5
		4	57.6	1788.1
		5	57.6	1746.4

Build	Raster angle	Sample	Yield strength (MPa)	Flexural modulus (MPa)
Vertical	0-90	1	73.8	2086.9
		2	76.9	2046.1
		3	75.9	2061.9
		4	76	2100.6
		5	74.3	2058.9
	45-45	1	66.5	1869.2
		2	63	1874.8
		3	65.3	1889
		4	67.4	1836.9
		5	66.8	1830.2

APPENDIX E.

MECHANICAL PROPERTIES OF SOLID BUILD COUPONS FOR VARIOUS BUILD PARAMETERS IN COMPRESSION TESTING

Raster width = 0.508 mm (0.02'); Temperature = 24°C

Build	Raster angle	Airgap (mm)	Sample	Yield strength (MPa)	Flexural modulus (MPa)
Horizontal	0-90	-0.00635	1	85.6	898.7
			2	85.9	840.1
			3	84.9	899.5
			4	83.8	889.2
			5	86.8	895.9
	0-90	-0.0127	1	87.6	899.1
			2	85.8	893.5
			3	85.1	895.3
			4	86.1	875.4
			5	86.8	897.8
	0-90	-0.01905	1	88.6	886.5
			2	84.7	903.7
			3	84.7	898.8
			4	87.3	903.3
			5	87.2	898.4
	45-45	-0.00635	1	85.8	874.3
			2	84.9	887.9
			3	85.8	886.6
			4	86.9	899.1
			5	85.4	874.2
	45-45	-0.0127	1	84.5	891.7
			2	87.1	892.1
			3	83.5	878.3
			4	88	922.1
			5	85.3	893.7
	45-45	-0.01905	1	87.8	896.6
			2	87.5	906.3
			3	84.8	890.3
			4	85.1	888.9
			5	86.7	881

Build	Raster angle	Airgap (mm)	Sample	Yield strength (MPa)	Flexural modulus (MPa)
Vertical	0-90	-0.00635	1	72.2	829.7
			2	71.6	839.1
			3	74	800.8
			4	72.2	832.2
			5	74.1	806.8
	0-90	-0.0127	1	73.5	799.3
			2	72.8	796.8
			3	73.4	834.7
			4	70.2	865.1
			5	75.7	802.2
	0-90	-0.01905	1	72.7	808.2
			2	76.5	806.1
			3	74.3	832.6
			4	72.1	825.9
			5	72.4	827.8
	45-45	-0.00635	1	66.3	754.5
			2	66.5	755.9
			3	66	714.6
			4	62.7	768.4
			5	65	726.6
	45-45	-0.0127	1	66.5	705.9
			2	66.8	760.1
			3	65.7	743.1
			4	65.4	738.8
			5	65	785.3
	45-45	-0.01905	1	66.6	736.8
			2	67.3	750.2
			3	64	776.5
			4	68.4	798.8
			5	64.3	708.7

APPENDIX F.

MECHANICAL PROPERTIES OF SPARSE BUILD COUPONS FOR DIFFERENT BUILD DIRECTIONS AND RASTER ANGLES IN COMPRESSION TESTING

Raster width = 0.508 mm (0.02’); Air gap = 2.54 mm (0.1’); Temperature = 24°C

Build	Raster angle	Sample	Yield strength (MPa)	Flexural modulus (MPa)
Horizontal	0-90	1	43.9	625.5
		2	46.5	627.6
		3	47.7	644
		4	46.4	652.2
		5	43.5	661.7
	45-45	1	46.3	643.5
		2	45.7	662.2
		3	47.1	649.1
		4	45.6	641.2
		5	46.6	651

Build	Raster angle	Sample	Yield strength (MPa)	Flexural modulus (MPa)
Vertical	0-90	1	36.2	547.2
		2	37.5	544
		3	35.9	539.1
		4	37.5	523.8
		5	37.6	564.6
	45-45	1	26.6	440.6
		2	26.3	443.3
		3	26.4	452.2
		4	24.8	439.7
		5	24.7	475.1

REFERENCES

1. Bagsik, A., Schoeppner, V., "Mechanical properties of fused deposition modeling parts manufactured with ultem 9085," *Proceedings of the ANTEC, Plastics: Annual Technical Conference Proceedings,* ANTEC 2011.

2. Bagsik, A., Schoeppner, V., Klemp, E., "FDM part quality manufactured with ultem 9085," *14th International Scientific Conference on Polymeric Materials,* Halle (Saale), 2010.

3. Lee, B.H., Abdullah, J., Khan, Z.A., "Optimization of rapid prototyping parameters for production of flexible ABS objects," *Journal of Materials Processing Technology,* 169, pp. 54-61, 2005.

4. Lee, C.S., Kim, S.G., Kim, H.J., Ahn, S.H., "Measurement of anisotropic compressive strength of rapid prototyping parts," *Journal of Materials Processing Technology,* 187, pp. 627-630, 2007.

5. Ognzan, L., Dejan, M., Miroslav, P., "Effect of layer thickness, deposition angle and infill on maximum flexural force in FDM built specimens," *Journal for Technology of Plasticity*, Vol.39, Number 1, 2014.

6. Raut, S., Vijaykumar, S.J., Nitin, K.K, Singh, T.P., "Investigation of the effect of build orientation on mechanical properties and total cost of FDM parts," *Procedia Materials Science, 3rd International Conference on Materials Processing and Characterization,* 6, pp. 1625-1630, 2014.

7. Panda, S.K., Padhee, S., Sood, A.K., Mahapatra, S.S., "Optimization of fused deposition modeling process parameters using bacterial foraging technique," *Intelligent Information Management,* Vol. 1, Issue 2, pp. 89-97, 2009.

8. Rayegani, F., Onwubolu, G.C., "Fused deposition modeling process parameter prediction and optimization using group method for data handling and differential evolution," *International Journal of Advanced Manufacturing Technology*, 73, pp. 509-519, 2014.

9. Anitha, R., Arunachalam, S., Radhakrishnan, P., "Critical parameters influencing the quality of prototypes in fused deposition modeling," *Journal of Materials Processing Technology,* 118, pp. 385-88, 2001.

10. Vasudevarao, B., Nataranjan, D.P., Henderson, M., "Sensitivity of RP surface finish to process parameter variation," *Department of Industrial engineering,* Arizona State University, 2010.

11. Park, H., Geoffrey, V., *Statistical Process Monitoring and Optimization*, Vol. 160. New York: M. Dekker, ISBN- 9780824760076, pp. 415-425, 2000.

12. Thrimurthulu, K., Pandey, M.P., Reddy, V.N., "Optimum part deposition orientation in fused deposition modeling," *International Journal of Machine Tools and Manufacturing,* 44, pp. 585-594, 2004.

13. Gurrala, P.K., Regalla, S.P, " Optimization of support material and build time in fused deposition modeling using central composite design methodology," *26th International Conference of CAD/CAM, Robotics and Factories of the Future.* Kuala Lumpur, Malaysia, 26-28 July, 2011.

14. Vijay, P., Danaiah, P., Rajesh, V.D., "Critical parameters affecting the rapid prototyping surface finish," *Journal of Mechanical Engineering and Automation*,Vol. 1, Number 1, pp. 17-20, 2011.

15. El-Gizawy, A.S., Corl,S., Graybill, B., "Process-induced properties of FDM products," *Proceedings of the ICMET, International Conference on Mechanical Engineering and technology Congress and Exposition,* Paris, France, ICMET 2011.

16. Croarkin, C., Tobias, P., "NIST/SEMATECH e-handbook of statistical methods," http://www.itl.nist.gov/div898/handbook/, Updated - April 2012.

17. Derringer, G., Suich, R., "Simultaneous optimization of several response variables," *Journal of Quality Technology*, 12(4), pp. 214-219, 1980.

18. ASTM International – D790-10, standard test methods for flexural properties of unreinforced and reinforced plastics and electrical insulating materials.

19. Buchan, E., "Stats direct: Statistical analysis – P-value", www.statsdirect.com/p_values**.**

20. ASTM International – D695-15, standard test for compression properties of plastics.

VITA

Krishna Prasanth Motaparti was born on September 4, 1991 in Chennai, India. In May 2013 he received his Bachelor's degree with honors in Mechanical Engineering from M.V.S.R. Engineering College, Hyderabad, India.

In August 2013 he joined Missouri University of Science and Technology to pursue his Master's degree in Mechanical Engineering. He was a graduate teaching and research assistant during his two and a half years of studies at the master's level. In May 2016 he graduated with a Master of Science degree in Mechanical Engineering